We are IntechOpen, the world's leading publisher of Open Access books Built by scientists, for scientists

4,800
Open access books available

122,000
International authors and editors

135M
Downloads

Our authors are among the

154
Countries delivered to

TOP 1%
most cited scientists

12.2%
Contributors from top 500 universities

WEB OF SCIENCE™

Selection of our books indexed in the Book Citation Index in Web of Science™ Core Collection (BKCI)

Interested in publishing with us?
Contact book.department@intechopen.com

Numbers displayed above are based on latest data collected.
For more information visit www.intechopen.com

2

Physiological Basis and Image Processing in Functional Magnetic Resonance Imaging: Neuronal and Motor Activity in Brain

Rakesh Sharma[1] and Avdhesh Sharma[2,3]
[1]*Amity Institute of Nanotechnology, Amity University, Uttar Pradesh, NOIDA*
[2]*Department of Electrical Engineering, Indian Institute of Technology Rajasthan, Jodhpur,*
[3]*Department of Electrical Engineering, Jai Narain Vyas University, Jodhpur Rajasthan, India*

1. Introduction

Functional magnetic resonance imaging or functional MRI (fMRI) is a type of specialized MRI scan used to measure the hemodynamic response (change in blood flow) related to neural activity in the brain or spinal cord of humans. Blood-oxygen-level dependence (BOLD) is the MRI contrast of blood deoxyhemoglobin, first discovered in 1990 by Seiji Ogawa at AT&T Bell labs and Functional Magnetic Resonance Imaging (fMRI) was soon introduced to map the changes in brain local blood flow, oxygenation or hemodynamics that correspond to regional neuronal activity of brain accompanying metabolic events [Ogawa et al. 1990]. Recent investigations focused on specific brain regional and functional specificity to delineate the specific distribution of neural activities at a given moment in the brain as a whole. It extended for brain anatomical imaging to map different structures and specific function of human brain. Present time, high resolution, noninvasive neural activity by a blood oxygen level dependent signal by fMRI has tremendous potentials for assessing the neurological status and neurosurgical risk [Tegeler et al. 1999; Lee et al. 1999; Singh et al. 2003; Bandettini et al. 2001]. Now fMRI applications have extended the understanding of neuronal and motor activities associated with different brain regional functions with additional information down to perfusion/diffusion of neurochemicals to cause neuroactivation. Presently, fMRI serves as non-invasive imaging and evaluation of neurophysiological/neuropsychological activities of brain that depend more on uncontrolled physiological motion in brain and functional characteristics of different locations such as cognition, sensory and motor active areas.

Present chapter serves a handful guide to practicing physician experts in fMRI. Functional magnetic resonance imaging (fMRI) is recently developing as imaging modality used for mapping hemodynamics of neuronal and motor event related tissue blood oxygen level dependence (BOLD) in terms of brain activation. In first section, we describe functional MR signal origin, physical basis of fMRI data generation, its physiological dependence on oxygen state in flowing blood and neuroactivation mechanism. In next section, image processing is described as performed by segmentation and registration methods. In next

section, segmentation algorithms are illustrated to provide brain surface-based analysis, automated anatomical labeling of cortical fields in magnetic resonance data sets based on oxygen metabolic state. In next section, registration algorithms are illustrated to provide geometric features using two or more imaging modalities to assure clinically useful neuronal and motor information of brain activation. In nutshell, present chapter introduces basic concepts of fMRI and reviews the physiological basis of fMRI signal origin and contrast mechanisms with state-of-art fMRI segmentation and registration algorithms to identify cortical visual response and event related cortical areas associated with neurophysiological measurements and potential image post-processing directions in future. In the end, the chapter summarizes the current developments in physiological basis of fMRI signal, its origin, contrast enhancement, physical factors, anatomical labeling by segmentation, registration approaches of visual and motor activity in brain with a review of clinical applications of fMRI in motor sensory functions, multiple sclerosis and Alzheimer's Disease to explore the other different neurophysiological and imaging modalities.

2. The physiological basis of fMRI

2.1 Basics

It became clear in last decade that fMRI signal is coupled or 'blood linked' with neuroactivation due to regional changes of blood flow and its redox oxygen state or ferric-ferrous ionic state in hemoglobin. Idea was roped up as 'neurophysiological' effect sensitive to fMRI signal is generated due to 'neuropsychological' activity in specific regions in brain. As a result, neurovascular and neurometabolic coupling (neurophysiological effects) establishes the critical link between a focal change in neuronal activity and MRI-detectable observations. In fact, all neuroactivation task performances such as arousal, attention, alertness, adaptation, sleep, or consciousness that affect the blood perfusion or vascular hemodynamics do interfere with oxygenation-sensitive mapping by fMRI techniques. Increased neuronal activity needs the metabolic oxygen support. For that, blood flow provides the metabolic substrates or energy rich neurochemicals. Still there is paucity of information of metabolic requirements and hemodynamic response in different brain cognitive functions. Historically, these cognitive observations initially were supported by reports on local reduction in deoxyhemoglobin due to increased blood flow without change in oxygen extraction [Zaini et al. 1996]. Conceptually, weak susceptibility effect induced by deoxyhemoglobin acts as paramagnetic endogenous contrast agent to represent neuroactivation (active perfusion) or label of oxygen oversupply and alters the T_2* weighted pixel intensity (functional magnetic resonance image signal) [Reber et al.2002; Preibisch et al. 1999; Nakai et al. 2001; Bandettini et al.2000] and serves as the source of the neuroactivation signal (fluctuation of SNR) for fMRI. Such fluctuations originate in fMRI as a result of 3D variations in spatial frequencies and line width (B) in x, y, z directions (gradients define location of neuroactivation and slice position). Other physiological factors such as physiological drifts (fluctuations of SNR, frequency distribution, signal intensities, BOLD signals) also participate. It is based on the fact that spatial distribution of low-frequency drifts in human brain follows a tissue-specific pattern, with greater drift magnitude in the gray matter than in white matter. In gray matter, the dependence of drift magnitudes on TE remains similar to that of task-induced BOLD signal changes. For

example, absolute drift magnitude reaches the maximum when TE approaches equal to T_2* whereas relative drift magnitude increases linearly with TE. By systematically varying the flip angle, drift magnitudes show a positive dependence on image intensity. Last decade was an excitement for clinical application of 3T-7T clinical scanners to observe functional activity of visual cortex using magnetic field susceptibility insensitive fast spin echo method [Turner et al.1993; Kwng et al. 1995; Russ et al. 2002; Miki et. al. 2001; Shibata et al. 2000; Fransson et al. 1997], the motor cortex [Kim et al. 1999; Mandeville et al. 1999; Toma et al. 2002; Kim et al. 1995; Nakada et al.2001] and Broca's area of speech and language-related activities [Kim et al. 1995; Nakada et al.2001]. fMRI and conventional neurophysiological techniques have been in use to localize the specific functions of the human brain [Logothetis et al.2001; Mayville et al.1999; Haslinger et al.2001; Kim et al. 2000; Ogawa et al. 1998; Jueptner et al. 1995]. Recent trend was focused on identification of brain regions involved with characteristic oxygenation-sensitive MRI response function. The art of other imaging techniques such as the neurochemical changes, chemical shift imaging, diffusion/perfusion dynamic imaging integrated with fMRI technique is in infancy. In next section, we describe the oxygen dependent nature of fMRI sensitive to neuroactivation and cerebrovascular blood flow.

2.2 Tissue oxygen content and framework for BOLD Signal

fMRI images can be made sensitive to local oxygen concentrations in tissue by choosing right MRI protocol. BOLD signal derives from the local concentration of deoxygenated hemoglobin that is modulated by several factors. The generator of this paramagnetic contrast agent is oxygen metabolism ($CMRO_2$). Blood oxygenation and blood magnetization both depend upon the balance of oxygen flow into and out of a region. The rate of oxygen inflow is proportional to cerebrovascular blood rate (CBR). During functional brain activation, increased CBF produces a washout of Hb_r as contrast agent by counteracting the effect of increased $CMRO_2$. Local blood volume fraction determines the deoxyhemoglobin content of a voxel at any level of blood oxygenation. As blood vessels swell, magnetic fields extend further into the brain tissue, causing a signal loss in the extravascular space. BOLD contrast can be approximated as changes in the BOLD relaxation rate scale with changes in the deoxy hemoglobin concentrations i.e. BOLD contrast (X) = K.A $[Hb_r]$, where 'x' depends upon the magnetic field strength and the sample volume.

A BOLD framework is based upon conservation of oxygen mass (Fick's Law) i.e. at the steady-state, unidirectional extraction of oxygen from the blood is the difference between the 'flow' of oxygen 'into' and oxygen 'out' of the volume, FO_2^{IN} -, FO_2^{OUT} = dV/dt. The resulting expression takes a form like the following:

$$\Delta R_2 = -K\,[Hb_r]_o\{\Delta F/F_o - \Delta V/V_o - \Delta M/Mo\} \quad (1)$$

F, V, and M refer to CBF, CBV, and $CMR0_2$ respectively. Subscript "o" indicates baseline values prior to stimulation. BOLD signal changes are positive when the quantity in brackets is positive.

Positive stimulus-induced BOLD represent the relative changes in CBF that exceed over combined effect of changes in CBV and $CMR0_2$. $[Hb_r]_o$ is proportional to V and M_o and

inversely proportional to F as shown in Figure 1 that combine to generate BOLD signal. Equation (1) stands good for small functional changes while intravascular signal contributions affect the linear relationship between ΔR_2, and $\Delta[Hb_r]$ dependence on blood oxygen and blood volume. The term $\Delta V/V_o$ is relative change in total venous hemoglobin.

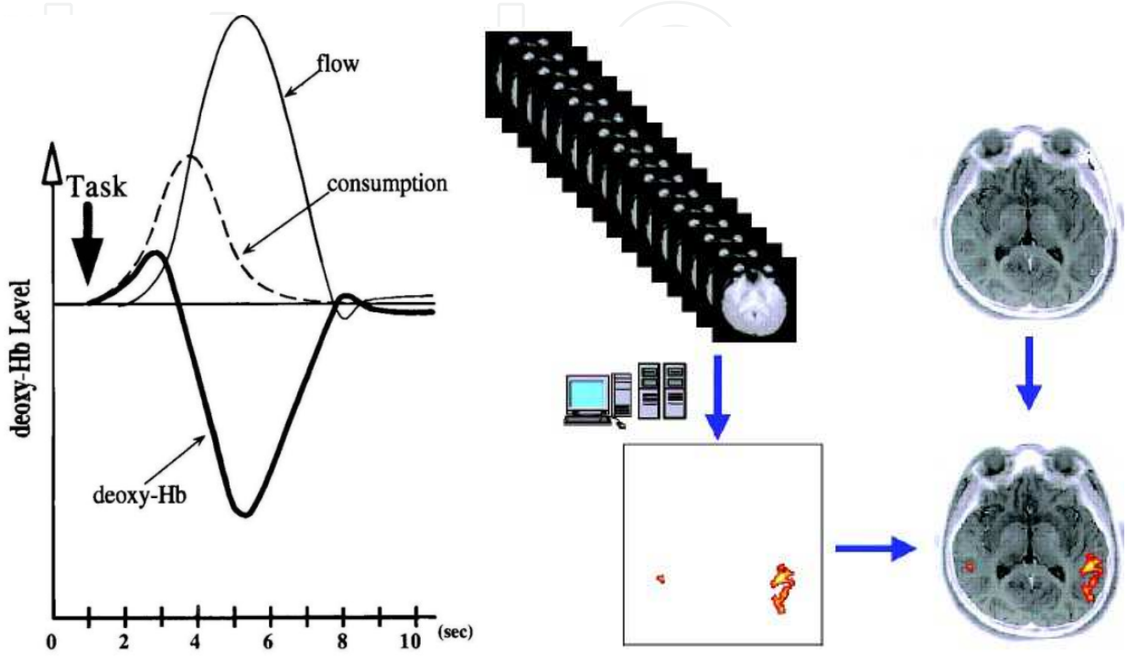

Fig. 1. Figure represents the "Oxygen oversupply" hypothesis. Regional deoxy-Hb (thick solid lines) decline is associated with increase in regional blood flow (thin solid line) and oxygen consumption (broken lines). In fMRI, T2* is described as blood flow based functional imaging of brain activation as sum of all activation pixels (yellow color) from all serial images shown in the figure (on right).

A rapid change in CBF produces an effect on BOLD signal that is both delayed and dispersed by transit through the vascular bed. The framework of Equation (1) of BOLD signal does not specify how oxygen is allocated, as long as the total amount is conserved. However, the quantities $\{\Delta F/F_o - \Delta V/V_o - \Delta M/M_o\}$ do not change arbitrarily during brain activation. The reproducibility of BOLD results across systems and BOLD stimuli poorly represent the coupling [Villringer et al.1999].

2.3 CBF and $CMRO_2$

Regional basal cerebral oxygen and glucose utilization show a molar ratio consistently less than $6(CMRO_2/ CMR_{glu} - 5.5)$, suggesting that the oxidative glucose metabolism ($C_6H_{12}O_6 + 6\ O_2 + 6H_2O + 6CO_2$) is the primary source of energy. Tight linear couplings have been shown for regional basal measurements of CBF versus CMR_{glu} and CBF versus $CMR0_2$ [Buxton et al.1997].

2.4 BOLD stimulus-induced neuroactivation and physiological changes

Blood oxygen is delivered to the brain by gaseous-fluid diffusion along an oxygen concentration gradient that falls in the neuroactivated brain tissue. As a result, specific brain region gets low oxygen reserves. So blood flow in that region experiences the increases of oxygen delivery or MR sensitive changes (temporal resolution) resulting with following effects: reduced blood transit time through the capillaries; decreased oxygen; extraction fraction; restricted capillary area; and vascular resistance at the local level. So, the regional trajectories represent the temporal physiological quantities determined from the baseline or average state i.e. the diffusion and regional coupling of CBF and $CMRO_2$ match during the brain activation. The current viewpoint of CBF-$CMRO_2$ coupling and regional relationship with rate of oxygen delivery explained the events during brain activation by Buxton-Frank diffusion-limited model of oxygen delivery [Zaharchuk et al.1999]. The exact scaling between relative changes in blood flow (f) = F/F_d and relative changes in oxygen delivery (M) depend upon the baseline value of the extraction fraction (E_o) and extent of capillary dilation as:

$$(v) = V / V_o \tag{2}$$

$$M = f\,(1 - (1 - E_o)^{v/f}) / E_o \tag{3}$$

Empirically, the influence of $CMR0_2$ on BOLD signal can be deduced by comparing the responses of CBF and BOLD signal using stimuli that affect CBF and $CMRO_2$ i.e. hypercapnia modulates CBF without changing oxygen-utilization. Focal activation of the human visual cortex increases $CMRO_2$ [31]. By using graded levels of visual stimulus and hypercapnia, a linear coupling was measured between relative changes in CBF and $CMRO_2$ for flow [Disbrow et al.2000].

2.5 CBF and CBV

Cerebral vascular resistance is defined as the 'total pressure drop' across a vascular bed. In the brain, intravascular pressure drops from mean arterial blood pressure in large arteries to venous pressure in the large veins. The brain activation increases CBF by reducing cerebral vascular resistance corresponding to an increase in CBV. Blood flow and blood volume both exhibit different temporal responses [Cheng et al.2001]. However, the basal blood level of deoxygenated hemoglobin is determined by the ratio of $CMRO_2$ to CBF. Neurophysiological changes in fMRI alter BOLD signal by resetting the ratio of basal $CMRO_2$ to CBF, and altering CBV [Cox et al. 1996].

2.6 Sensitivity of fMRI signal

Blood volume fraction, oxygen extraction fraction, distribution of vessels, arterial oxygenation neurophysiological factors and intravascular or extravascular signals depend upon the applied MR pulse sequence, field strength, degree of neuroactivation and the physiology of the functional variable etc. Sensitivity is the product of the relative change in brain 'activation' (flow, volume, oxygenation, etc.) and 'amplification' factor expressing the intrinsic sensitivity per unit change:

$$\text{Sensitivity} = (\text{activation}) \times (\text{amplification}) \quad (4)$$

The amplification factor applies spatial resolution to the pattern of brain activation but it is independent of the degree of activation [32]. For detecting changes in local brain functional activity, fMRI signal-to-noise ratio (fSNR) refers to the time-averaged value of signal divided by the temporal standard deviation of the signal: $fSNR = S_t/\sigma_t$.

Similarly, contrast for fMRI or functional CNR per unit time (fCNR) may be expressed as the ratio of time dependent signal changes (δS) to time-dependent noise:

$$fCNR = \delta S_t / \sigma_t, fSNR \times \delta S_t / S_t \quad (5)$$

3. Basic functional MRI sequences and physical factors of functional MRI contrast

In routine, fast Flow Attenuated Short Echo (FLASH) or single-shot EPI pulse sequences with prolonged echo times are employed depending on the desired spatial or temporal resolution. These pulse sequences are shown in Figure 2. Typically, EPI sequences acquire all differently phase-encoded gradient echoes required for image reconstruction after a single slice-selective RF excitation pulse. The individual echoes are generated by multiple sinusoidal or trapezoidal reversal of the read or frequency-encoding gradient. Phase encoding is performed by a 'blipped' gradient, whereas the EPI technique uses a 'weaker' constant gradient. Echoes cover a large range of different echo times. The effective TE is given by the Fourier line representing the lowest spatial frequency, i.e. for zero phase encoding, as it dominates the image contrast. Basic emphasis is on high speed yield and image acquisition times of the order of 100 ms and excellent maximum volume coverage by multi-slice fMRI imaging at the expense of limited in-plane resolution.

In contrast, FLASH sequences require multiple RF excitations with low flip angles < 90° that normally generate only a single gradient echo per repetition interval. As large TE values also prolong the repetition time, typical imaging times are in the range of several seconds. The ability to select an arbitrary compromise between temporal and spatial resolution is best exploited for gaining access to high-resolution maps at the expense of less volume coverage. However, EPI images also suffer from several unavoidable artifacts. In following section, we describe different brain areas to correlate distribution of fMRI pixel intensities with cognitive functions as guideline to neuropsychological geography of brain.

4. Neuropsychological geography of neuroactivation in brain

Recent trend in fMRI research was to understand the relationship of physiological mechanisms and selective activation of different brain locations using fMRI techniques. However, the knowledge of the independent brain functions and control by different parts is still in infancy. fMRI has long way to answer the physiological stimuli and mechanism of different fMRI BOLD signals. The success of it solely depends on power of fMRI image processing. Recent investigations highlight the fMRI visible different brain areas as shown in FIG 3, new understanding of fMRI sensitive physiological stimuli and use of high field scanners.

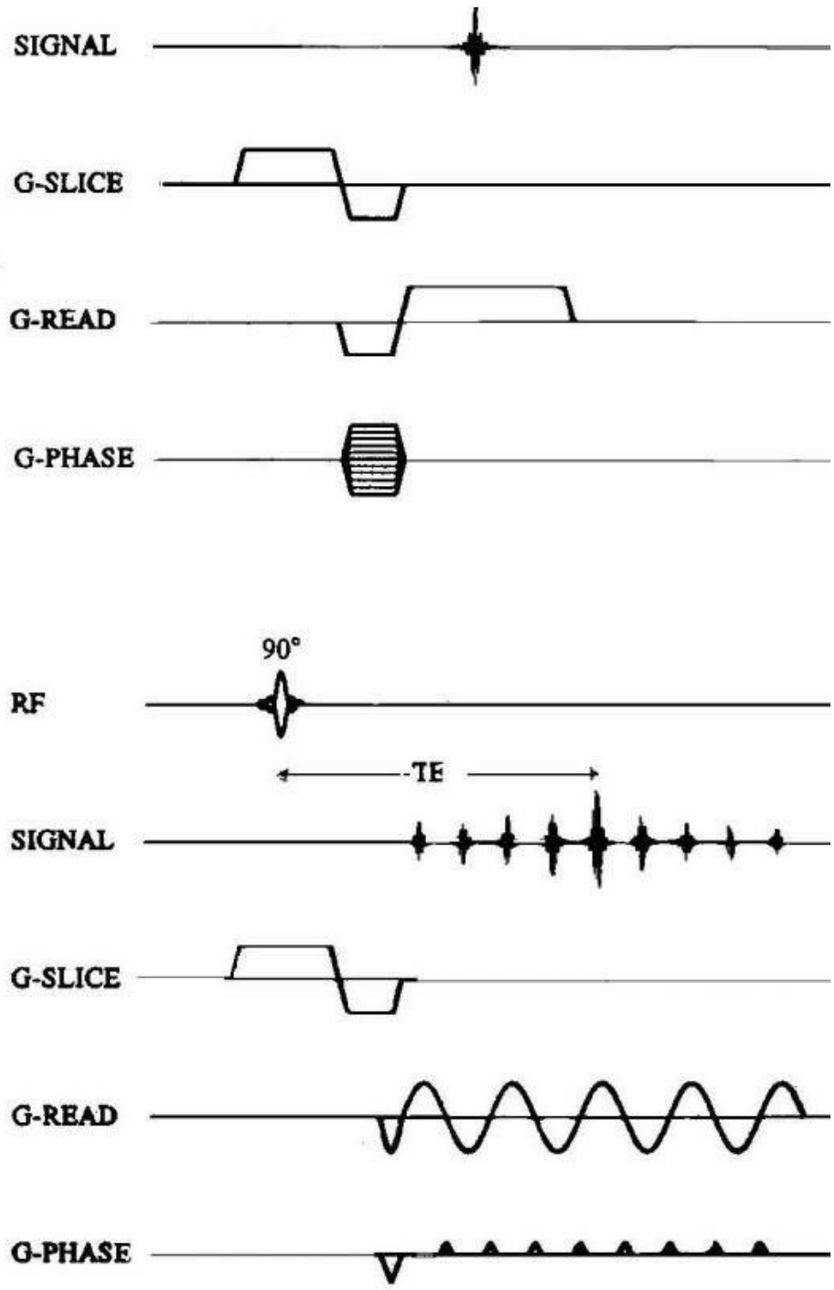

Fig. 2. A basic EPI sequence FLASH (top) and single-shot EPI Sequence (bottom) for functional Imaging is shown with reversible reading gradients and pulses to generate rapid images in less than a minute.

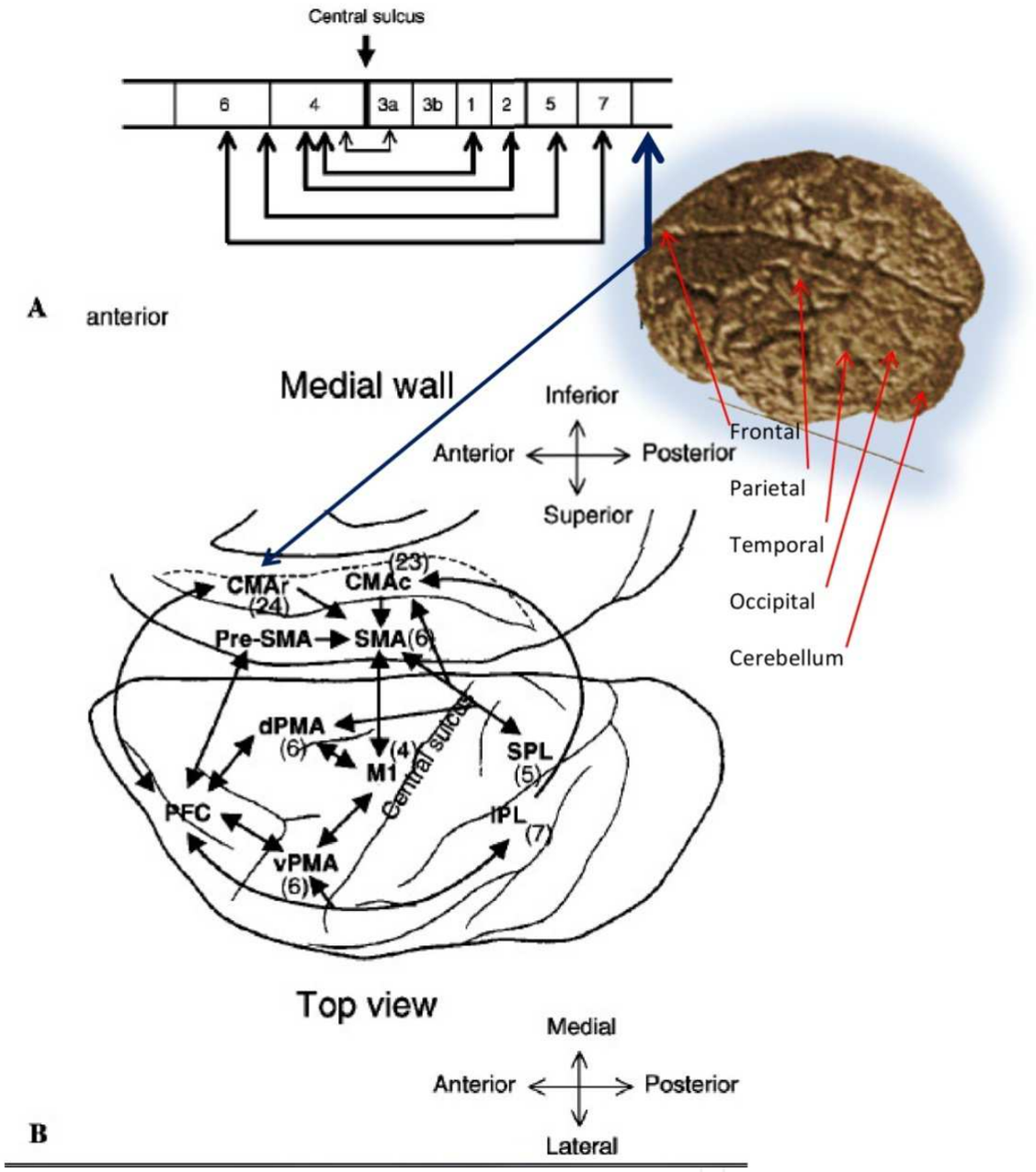

Fig. 3. An illustration of anatomical connections between motor areas are shown. A: A sagittal section of gray matter shows reciprocal organization of frontal motor and parietal sensory cortices with respect to the central sulcus. Brodmann's area (BA), reciprocity between rimary areas (BA4 and BA3, 1 and 2 and reciprocity between nonprimary areas (BA6 and BA5 and 7) are shown by arrows. B. Interconnections between multiple motor-related cortices are represented with numbers in parentheses. These are: Brodmann's area M1: Primary motor cortex, SMA: Supplementary motor area, dPMA: Dorsal premotor area, vPMA: Ventral premotor area, CMAr: Rostral cingulated motor area, CMAc: Caudal cingulated motor area, PFC, Prefrontal cortex, SPL: Superior parietal lobe, IPL: Inferior parietal lobe.

5. Validation and physical factors in functional MRI

BOLD and fMRI characteristics are important determinants in validation process of ultrafast fMRI image acquisition of raw data and 'task to functional map' correlation by postprocessing and statistical analysis. We describe these concepts that validate brain activation, fMRI spatial resolution and BOLD events. Two assumptions support the validation of fMRI to pick up brain activation signal: 1. Any motor or sensory action of body generates specific motor or sensory response in neural circuit with a result in cerebrovascular blood flow change due to oxygen state in flowing blood; 2. 'Brain activation' is read as 'statistically significant pixel intensity changes' associated with a given set of tasks to denote the area of neuronal activation. It is a scalar number given by MRI system upon completion of image reconstruction including magnetic correction and other inherent factors. MRI spatial resolution is low in the range of 4 mm^3 on high field MR scanners. BOLD events are neuronal events. T2* contrast changes seen in fMRI are an empirically observed biological phenomenon. For fMRI, T2* contrast is 'weak' susceptibility effect of deoxy-hemoglobin (deoxy-Hb). In following sections we describe some known physical factors responsible of functional MRSI (task→oxygen change in blood Hb→change blood flow→brain activation→pixel intensity change→3D Talairach maps and changes in metabolites). Some known intrinsic and extrinsic factors are described to influence fMRI contrast in flowing section.

5.1 Susceptibility effects and T_2* contrast

In MRI, regional magnetic field inhomogeneity is common problem due to high paramagnetic susceptibility, ferromagnetic susceptibility and presence of air sinuses in brain, and B_o inhomogeneity. The susceptibility effect may affect a large area of the image matrix and can introduce image deformity. The smaller susceptibility effects introduce the pixel intensity changes in nearby pixels generating the T_2* contrast. This is the basis of fMRI that represents a 'statistical' method based on pixel intensity changes in the brain placed in high magnetic field B.

5.2 Magnet shimming

MRI is performed grossly by using high order gradient 1st and 2nd order shim coils to correct B_o inhomogeneity. Human brain undergoes the continuous motion and it makes hard to shim i.e. the line width of human brain is 200–400 Hz. Slice thickness and slab size over that focused shimming reduces the inhomogeneity. Fast spin echo (FSE) images are insensitive but echo planar images (EPI) are sensitive to inhomogeneity. In fMRI, selective RF excitation pulse applied through a gradient selects the appropriate slice thickness with appropriate inter slice gap between the slices.

5.3 Nyquist ghost

The unique k-space trajectory of the EPI sequence results in the appearance of a characteristic artifact termed 'Nyquist ghost'. However, in practice the most common cause of Nyquist ghost is minor field perturbation as shown in Figure 3. Nyquist ghost represents the fictitious activation encountered in fMRI. Direct adaptation of such paradigms to fMRI typically introduces task-correlated Nyquist ghost and fictitious activation.

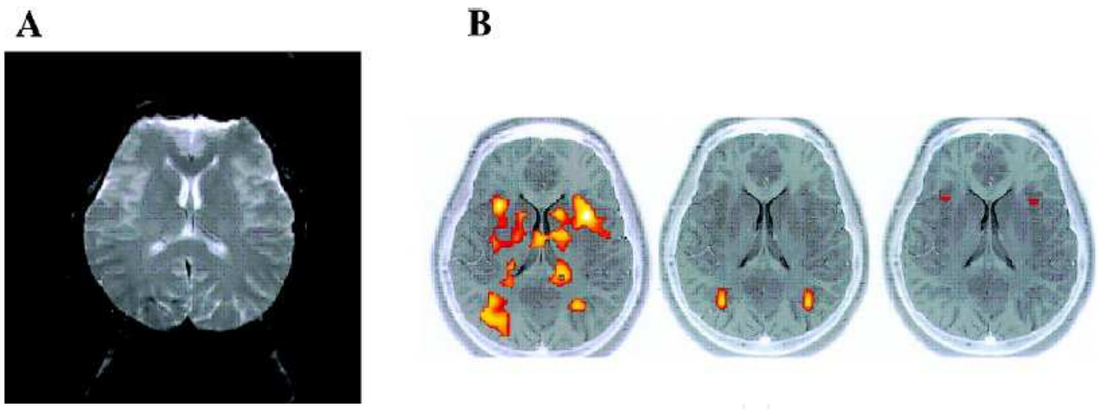

Fig. 4. The figure represents Nyquist ghost in panel A and representative fictitious activation in panel B. Notice the background bright signal as ghost (panel A) and activation areas (panels B) shown in yellow color spots which are not due to brain activation.

5.4 Pixel misalignment and limitation of spatial resolution

Pixel misalignment causes the fictitious activation due to subject motion as shown in Figure 4. Many "motion correction" post-processing algorithms have been developed based on the two-dimensional imaging and three-dimensional misalignments[Goodyear et al.2001; Kim et al. 2000; Kiebel et al. 2004]. The theoretical limit of the spatial resolution for fMRI is approximately 4 mm^3. fMRI image of the normal brain can be used to evaluate the relative intensity of cerebral cortex at various sites relative to CSF as shown in Figure 4. The substantial variation in the intensity of cortex is primarily due to the partial volume phenomenon as shown in Figure 5. The correction algorithms such as 're-slicing', 'standardization', or 'motion correction' image-processing methods as shown in Figure 6 have been reported [Meinzer et al.2011]. Basically, each raw image data is used for statistical analysis. In the following description, some representative examples of application of these physiological principles of fMRI are illustrated.

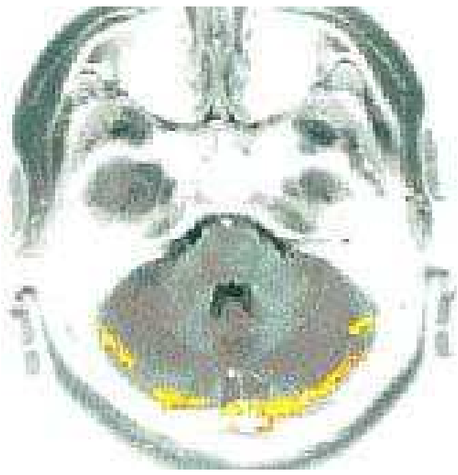

Fig. 5. The figure represents fictitious activation due to pixel misalignment. The bright spots around the bottom brain surface are misaligned that create illusion of active areas shown in yellow color.

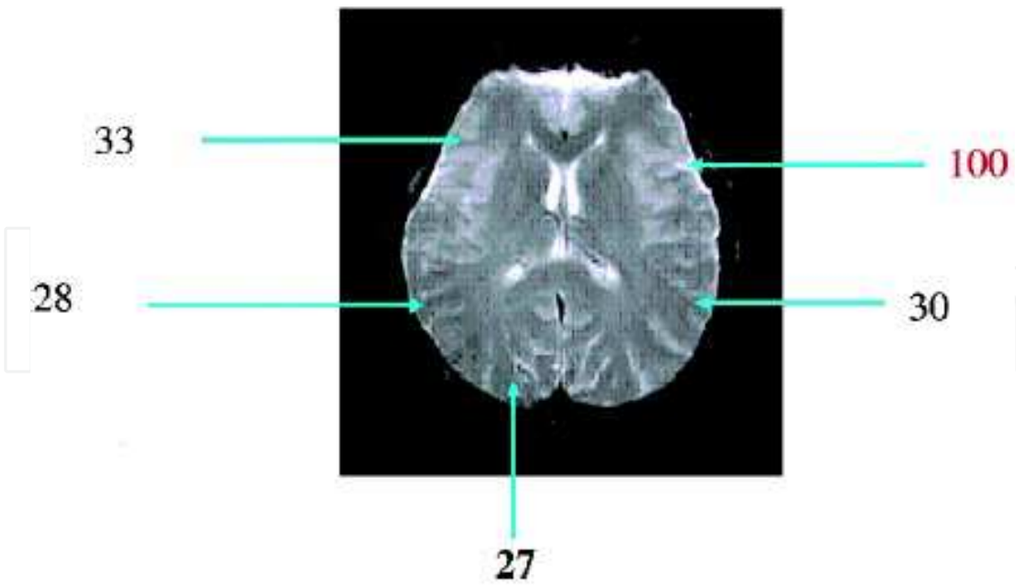

Fig. 6. An example of an fMRI image of the normal brain is shown. The numbers indicate the relative intensity of cerebral cortex at various sites relative to CSF which assigned a value of 100 (written in red). The substantial variation in the intensity of cortex is primarily due to the 'partial volume' phenomenon.

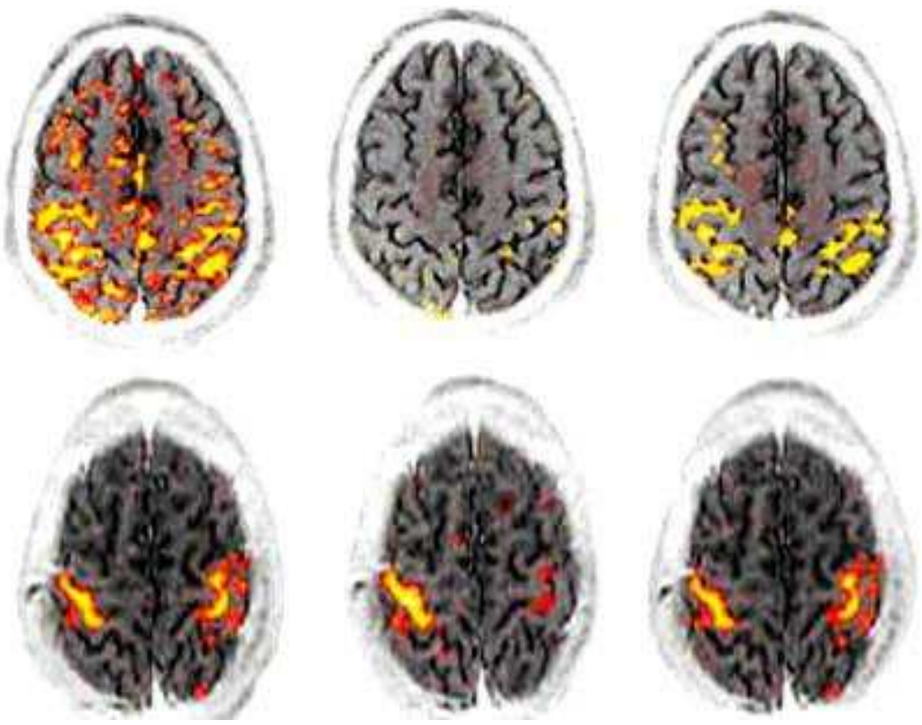

Fig. 7. The figure illustrates the effects of motion correction algorithm SPM 96. The activation maps were obtained for a bilateral hand motion paradigm using a horizontal 3 T MRI system with image voxel resolution of 3 mm × 3 mm × 5 mm. In this setting, acceptable pixel misalignment was determined to be 0.6 mm. Brain motion exceeding

0.6 mm (> 0.6 mm) produced significant pixel misalignment artifact. A motion correction algorithm wiped out these artifacts as well as actual activation. It also wiped out a small cluster of fictitious activation, while 'true' activation remained visible. In contrast, brain motion less than 0.6 mm provided activation maps of bilateral primary motor cortices. Application of motion correction algorithm artificially eliminated true activation areas.

Functional MRI is sensitive to some sensory and motor response functions. In following section, we illustrate visual response function in relation with fMRI.

5.5 The vision response function

The oxygen concentration in brain serves as a tool to map cortical regions responsible for performing various cognitive tasks because oxygenation level in active cortex changes between baseline and tasking conditions i.e. pattered lights protocols affect the spatiotemporal response and characteristics in the visual system. These visual stimulations generate the signal rise due to differences between tonic and phasic MRI hemodynamic responses after the onset of activation i.e. rapid rise in BOLD response due to rapid increase in the blood flow or enhanced oxygen delivery / oxygen consumption. Recently, the delayed upregulation of oxidative glucose consumption in brain and a slow venous blood volume (balloon model) suggested them as two processes. These were relevant for fMRI mapping studies with shorter protocol timings [Villringer et al. 1999]. The link between neuronal activity and blood flow characteristics forms the basis for functional mapping using fMRI. These characteristics such as cerebral blood flow (CBF), cerebral volume (CBV), metabolic regional oxygen ($CMRO_2$), and BOLD signal form an interconnected set of quantities that are coupled during normal brain activation. For details, readers are suggested to read chapter 9 in this book.

5.6 Neurophysiological factors in functional MRI contrast

In this section, we describe various measures currently used to identify the activated pixels in corresponding fMRI maps i.e. analysis of signal differences, variances, statistical parameters, temporal correlations or frequencies, principal components, clusters, phase information, and noise characteristics. In visual response, time-locked averaging of images and subsequent subtraction across the functional states i.e. summation of images was reported that was acquired during one condition (e.g. lights off) and subtraction of the result from that obtained for a different condition (e.g. lights on) [Cox et al.1996]. This robust and sensitive approach exploited the temporal structure of the known stimulation protocol and compared it to the oxygenation-sensitive MRI signal intensity time courses, on a pixel-by-pixel basis. This 'boxcar' function was employed to calculate the color-coded activation map for correlation coefficients identifying the activation centers and optimum area delineation i.e. retinotopic maps on brain V1, V2, V4 and MT (visual cortex) measured by fMRI for establishing the accuracy of visual maps as basis of hemodynamic responses in these two cortical areas [Cox et al.1996]. The stimuli used block-alternation design with relatively long intervals of stimulus vs rest state. However, fMRI has been widely used to image ocular dominance and orientation columns within a fraction of a millimeter [Goodyear et al.2001; Kim et al.2000; Kiebel et al. 2004].

5.7 Functional MRI signal of motor and visual stimulation

In following section, two common examples of fMRI experiments of motor and visual stimulation are described. Before details of fMRI experiments, a brief description is given on fMRI anatomical geography to correlate different language regions in brain with their functional neuropsychological activities. Readers are requested to read neuroanatomy for further details.

5.8 Neurostimulus in aphasia and fMRI

Functional MRI can map changes in brain functionality at different Brodmann and Broca areas following a treatment to assess its effectiveness as neuroimaging-guided rehabilitation neuroscience [Meinzer et al. 2011]. Broca's area "classical language area", supports various tasks related to memory, music [Maess et al. 2001; Patel 2003], calculation, object manipulation [Binkofski et al. 2004], motor imagery [Binkofski et al.2000], perception of meaningful but not meaningless sequences of hand and mouth actions [Fadiga et al.2006a; Fadiga et al.2006b], time perception, rhythmic perception, processing of complex geometric patterns [Fink et al.2006], prediction of sequential patterns, and so on. Major functions are: (a) selection of information from competing sources [Thompson-Schill 2005], (b) a broader cognitive control function [Novick et al.2010], (c) language specific linearization of hierarchical language dependencies [Greewe et al.2005], (d) processing of hierarchical dependencies like those found in language and musical syntax [Optiz et al. 2007] involving cognition, perception, and action. The syntactic subsystem, which too contributes to auditory comprehension, is supported by Broca's area (BA) [Fink et al. 2006; Thompson-Schill 2005], the angular gyrus (BA 39), the supramarginal gyrus (BA 40), the superior temporal gyrus (BA 22), involving also the white matter structures, such as the basal ganglia [Kutas et al. 2000; Caplan et al. 2000]. The dorsal stream in its posterior part involves a portion of the Sylvian fissure at the parietal-temporal boundary, supporting the sensory-motor interface. Its anterior portion in the frontal lobe includes Broca's area and its vicinity, while its more dorsal premotor component "corresponds to the portions of the articulatory network" [Hickok et al. 2007]. The ventral stream in its posterior portion (posterior middle and inferior portions of the temporal lobes) supports linking of phonological and semantic information (the lexical interface), while its more anterior areas support the combinatorial network. Phonological subsystem supporting auditory comprehension activates certain temporal areas as well as the dorsal region of Brodmann area (BA) 44. The semantic level of auditory comprehension is also distributed; e.g., passive listening activates temporal region BA 22/42 bilaterally, while other semantic tasks may activate left BA 47, BA 45/46 and BA 44 [Friederici 1998].

Together with structural and other functional neuroimaging methods as well as with new observer-independent methods of cytoarchitectonic analysis [Amunts et al.2003], fMRI has created a new picture of Brodmann area. Downing & Peelen (2011) have contradicted that the body areas in the occipitotemporal cortex (OTC) do not actually support processing of the body itself (as a category), but rather its shape and posture (that is, its features), forming a perceptual network that also supports processing in other cortical systems "overlapping and segregated system for object representation" (p. 9) in the ventral visual cortex for fronto-parietal activation [Peelen et al. 2011]. New fMRI evidences indicate activations of

perilesional areas associated with small stroke lesions, while larger stroke lesions induce activation of the homologue areas in the opposite hemisphere [Cao et al. 1999]. A best example is Aphasia.

Much explored language disorder is Aphasia caused by brain damage due to a stroke, traumatic brain injury, tumour, atrophy and other neurological conditions. Neuroplasticity of brain can be associated with all aphasic types. Aphasia further can be divided into non-fluent (such as Broca's aphasia, transcortical motor or global aphasia) and fluent aphasias (e.g., Wernicke's aphasia, anomic and transcortical sensory aphasia). fMRI provides information on the remaining functionality of the injured brain after aphasia, involvement of other brain areas "taking over" the other brain functions, and the reorganization processes at work. To evaluate the "taking over" function, block design is used during blood oxygenation level-dependent (BOLD) fMRI based on "the temporal dynamics of the hemodynamic response delay" where increased blood flow remains 4 or 8 seconds after the response" to allow data collection after the task and "during the silent period of no speech, minimizing motion artifact from overt speech". Such neural activity involves Broca's area and the posterior perisylvian network (including Wernicke's area, the angular and supramarginal gyri), and RH homologues of these regions, plus the occipital area as a control area. Time to peak (TTP) data contain valuable information on patients' response to treatment, because changes in TTP reflect changes in the amount of time that a patient spends on a task from presentation of stimulus to verbal response. Brain cannot reorganize syntax after injury to left BA 45/47 and that the capacity of Right Hemisphere takes over function critically depends on the type of language function.

5.9 Visual stimulation and fMRI

The typical BOLD time course (shown in black) shows 4 'active' states and 4 'resting' states are shown in Figure 8. With prior knowledge of the activation timing (shown in red), a statistical test is performed on the data to determine active areas of the brain. In brief, MP-RAGE (magnetization prepared, rapid acquisition gradient echo) sequence generates a 3D anatomic image of the head and brain. fMRI is performed with T2*-weighted gradient recalled EPI. The visual stimuli are created on a visual stimulus generator graphics card. The stimuli are presented as dichoptic signals using polar filters and adjustable right-angle prisms for optical superimposition of the right and left image are shown in Figure 8. The stimuli appear as 'radial checkerboards', in which the high-luminance contrast checks exchanged position as a sinusoidal function of time. During rest (baseline) periods, subjects view a small black fixation mark superimposed onto a homogeneous field. The experimental paradigms contain five different epochs: Alternating monocular stimulation [A]; Simultaneous binocular stimulation [B]; left eye leading-right eye trailing [LR]; Right eye leading-left eye trailing [RL]; and baseline. Each rest epoch is followed by one of the described epochs of checkerboard stimulation. The complete sequence of one repetition is shown in Figures 8 and 9. In a recent report, BOLD contrast in visual cortex related to binocular interactions in primary visual cortex could be revealed by fMRI at high field 4 T MRI. Binocular and monocular stimulations were characteristic of high contrast radial checkerboard pattern-stimulated neurons tuned to high and low spatial frequencies. The different striate cells in ocular dominance columns interacted when they are simultaneously activated and reduced by binocular or monocular stimulation resulting with increased

BOLD response [Cao et al.1999]. However, binocular rivalry due to disparity appears as a source of error. Fixation of eye and maintaining it throughout scan period reduces the disparity which otherwise is commonly observed in area V3 by random-dot stereogram.

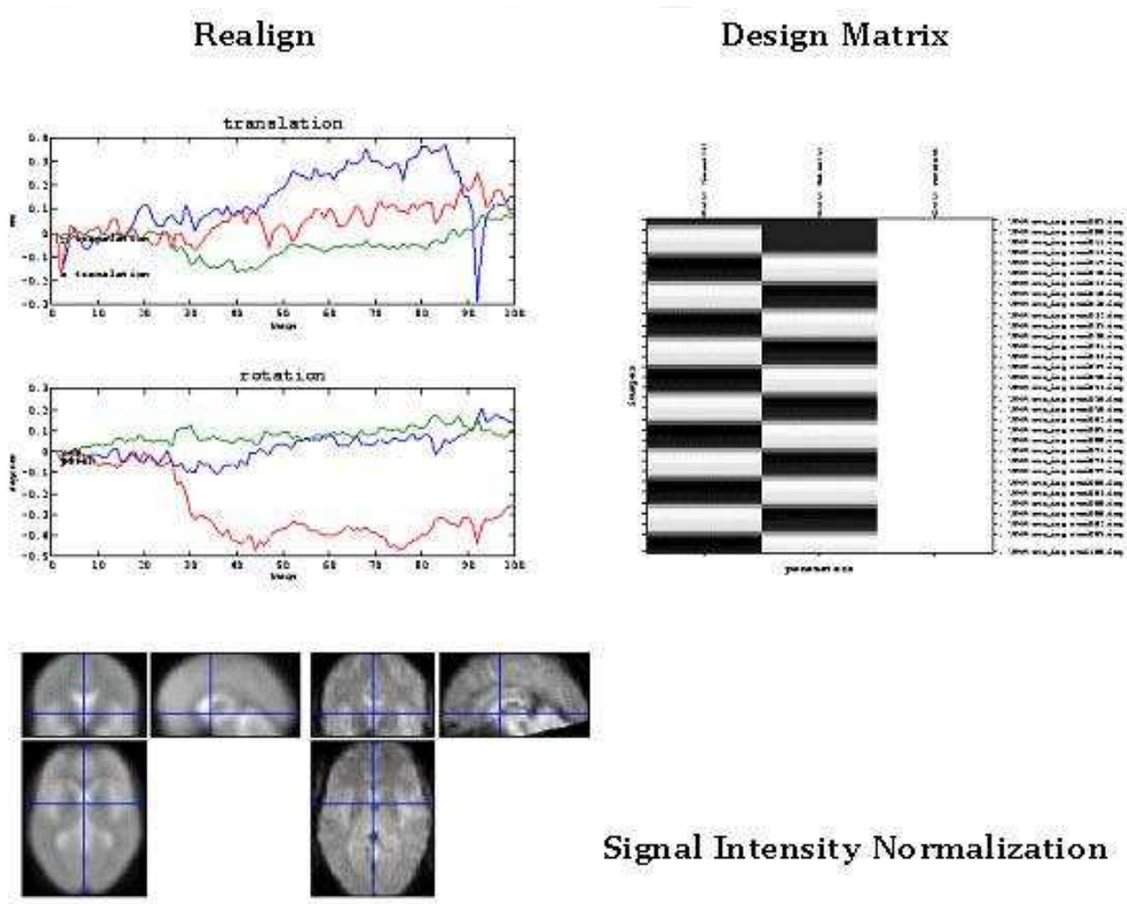

Fig. 8. Time course of activation for the four stimulus epochs (B binocular, M monocular RL right eye stimulated first, followed by left eye stimulation, LR left eye stimulation first, followed by right eye stimulation)(left panel). During stimulation period, the subjects perceived a single flickering radial checkerboard, whereas during the rest period they viewed a single black fixation mark at constant mean luminance (right panel). Typical time courses from region of interest (ROI) centered in one hemisphere in the primary visual cortex (VI) or in an extrastriate region. Statistical parametric maps of significant BOLD responses to alternating monocular stimulation compared to the binocular condition (right panel). Voxels in bright regions indicate strong response to alternating monocular stimulus. The cross hairs represent the most active voxel within the cluster used for normalization (bottom panels).

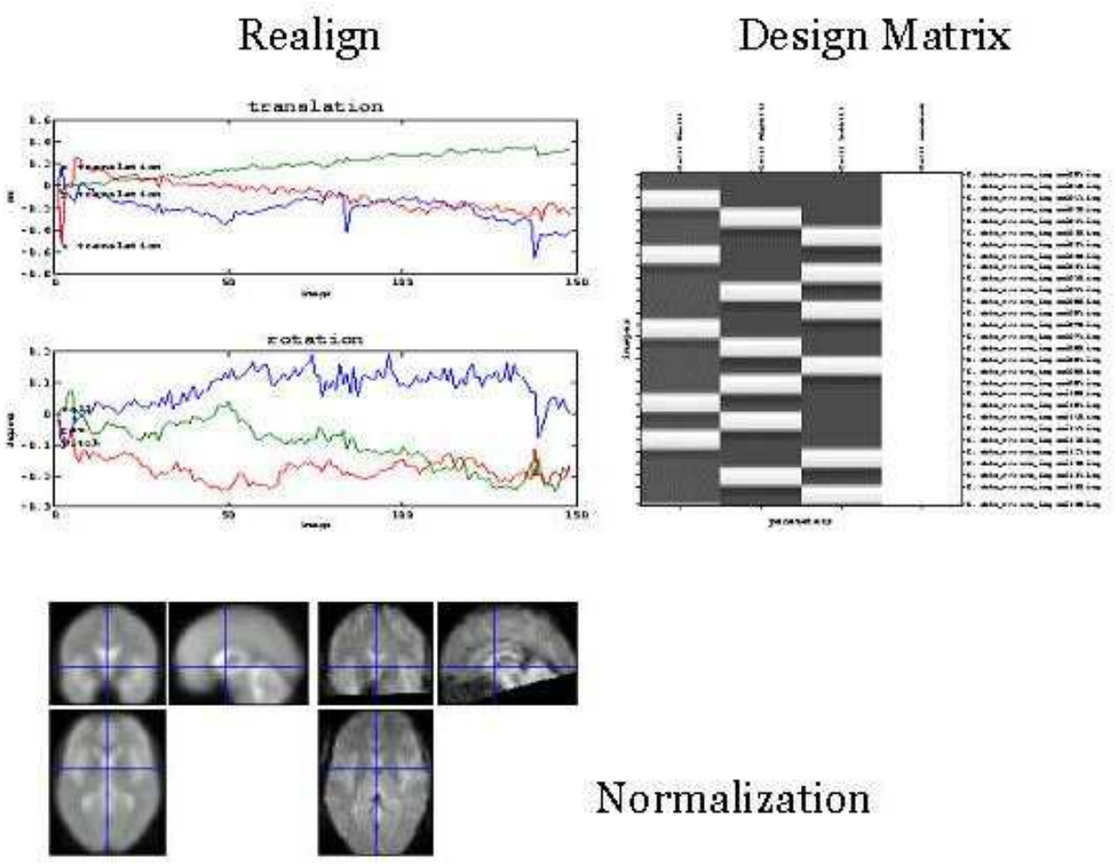

Fig. 9. Time course of activation for the four stimulus epochs (B binocular, M monocular RL right eye stimulated first, followed by left eye stimulation, LR left eye stimulation first, followed by right eye stimulation)(left panel). During stimulation period, the subjects perceived a single flickering radial checkerboard, whereas during the rest period they viewed a single black fixation mark at constant mean luminance (right panel). Typical time courses from region of interest (ROI) centered in one hemisphere in the primary visual cortex (VI) or in an extrastriate region. Statistical parametric maps of significant BOLD responses to alternating monocular stimulation compared to the binocular condition (right panel). Voxels in bright regions indicate strong response to alternating monocular stimulus. The cross hairs represent the most active voxel within the cluster used for normalization (bottom panels).

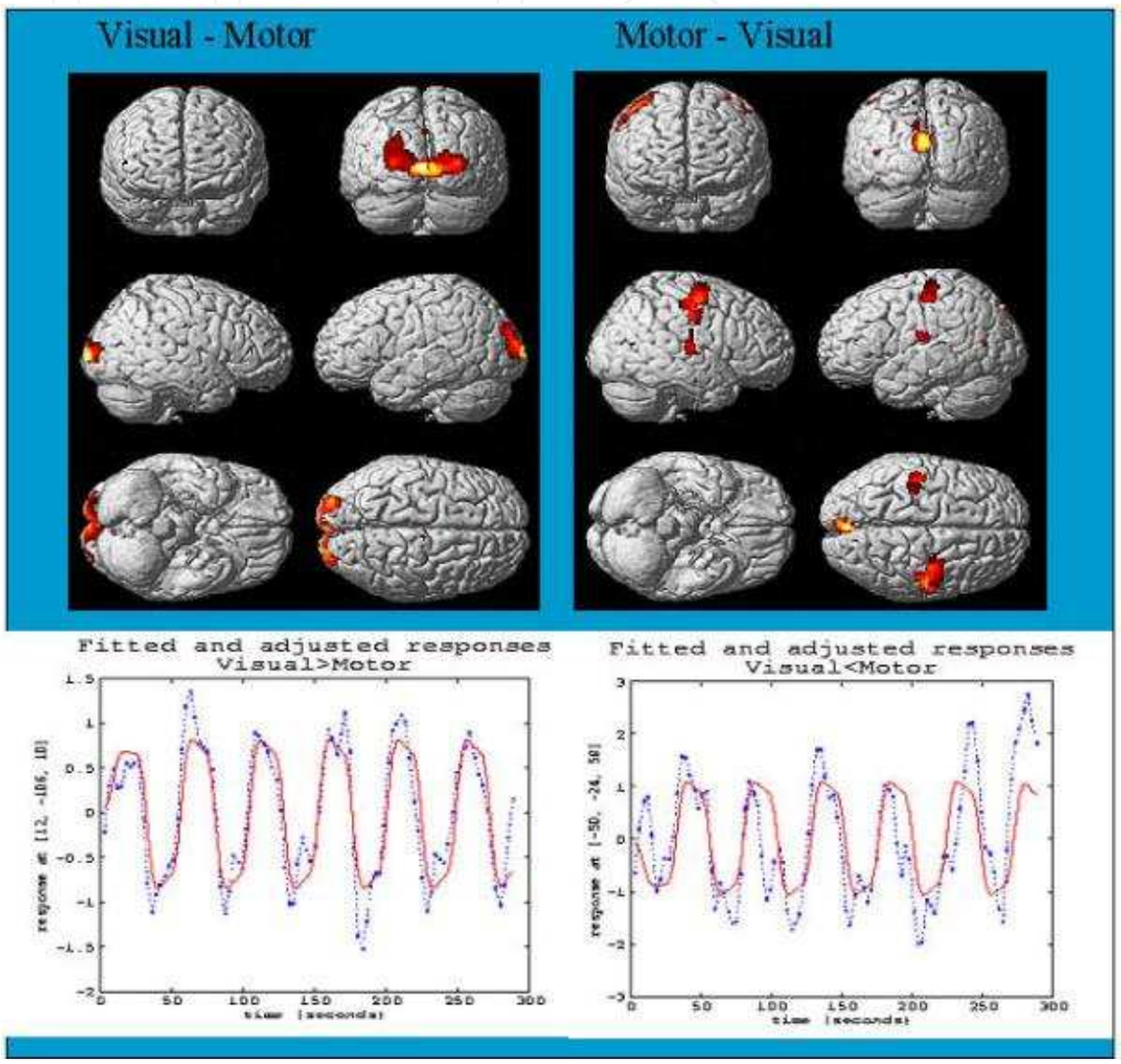

Fig. 10. Selected brain regions showing the activation areas observed by fMRI during finger movement. Regions with Z-score higher than threshold of 3.5 are displayed in red color. Stroke occurred in area colored as yellow. The time-course of on-off fMRI signal recorded in a typical voxel responding activation due to the stimulus paradigm (shown as red bold line).

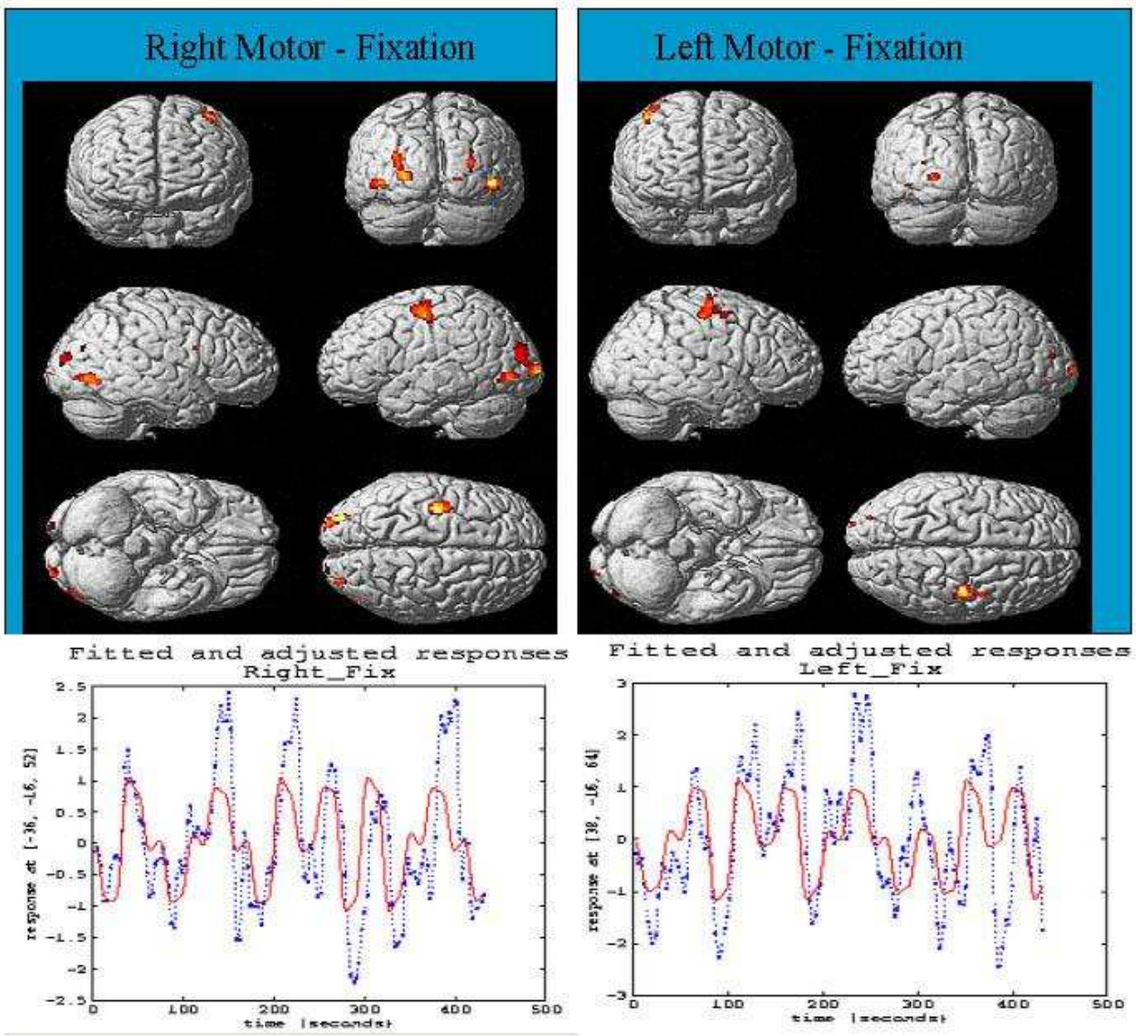

Fig. 11. Selected brain regions showing the activation areas observed by fMRI during finger movement. Regions with Z-score higher than threshold of 3.5 are displayed in red color. Stroke occurred in area colored as yellow. The time-course of on-off fMRI signal recorded in a typical voxel responding activation due to the stimulus paradigm (shown as red bold line).

5.10 fMRI activation in primary motor and pre-motor regions

Paralyzed patient retains the motor control. fMRI shows the activation in primary motor and premotor regions. An example is illustrated here for event-related finger tapping fMRI image acquisition and analysis. Right-handed subjects paralysed with eye blinking and restricted mouth movement with intact cognition were imaged by fMRI single-shot gradient recalled echo-planar imaging pulse sequence. Patients were simulated for the action of tapping fingers 'stimulus paradigm' as shown in Figure 10. Multiple regressions were applied to do statistical data analysis. Individual variables included 'box-car activation paradigm' and constants for activation signals. A ramp-regressor was used to remove linear-

drift in the signal. Standard deviated Z-score map was superimposed on high-resolution anatomical image to display brain activation areas. Time course signal in each voxel was obtained to reveal hemodynamic response to the stimulus paradigm. The regions of activation were mainly in contralateral to the primary motor area (M1) and premotor regions (PM) in right motor cortex with little activation in supplementary motor area (SMA). However, ipsilateral activation in premotor (PM) area of left motor cortex was also observed. The time series of functional MRI signals from the voxel in labeled areas (see Figure 11). The time series corresponded with activation paradigm suggesting time-course on-off binary fMRI signal by simulated motor task due to neuronal or cognition activity. It suggested the association of motor cortex, somatosensory cortex and visual cortex with cerebellum through pontine nuclei during its motor activity and rCBF increases.

5.11 3D motion paradigm subtractive approach

It generates activation fMRI maps significant for evaluation of symmetry of activation in the frontal lobes. The cerebrum cortex is not motion physiology sensitive (see Figure 12) but cerebellum cortex is motion physiology sensitive so pixel intensity changes represent its true activation maps as shown in Figure 13. However, paradigm independent structures with high susceptibility effects, partial volume effect become apparent on simultaneously FSE and EPI images as shown in Figure 14. Common examples are air sinuses, air spaces, and ferromagnetic substrates. It is the reason coronal images are not acquired for fMRI imaging but axial images show specific task-related activation areas. The figure shows activation in the right intrapareital sulcus of cerebrum cortex lobes (as arrow). The raw image fMRI image did not show ghost or susceptibility effect to cause fictitious activation. After

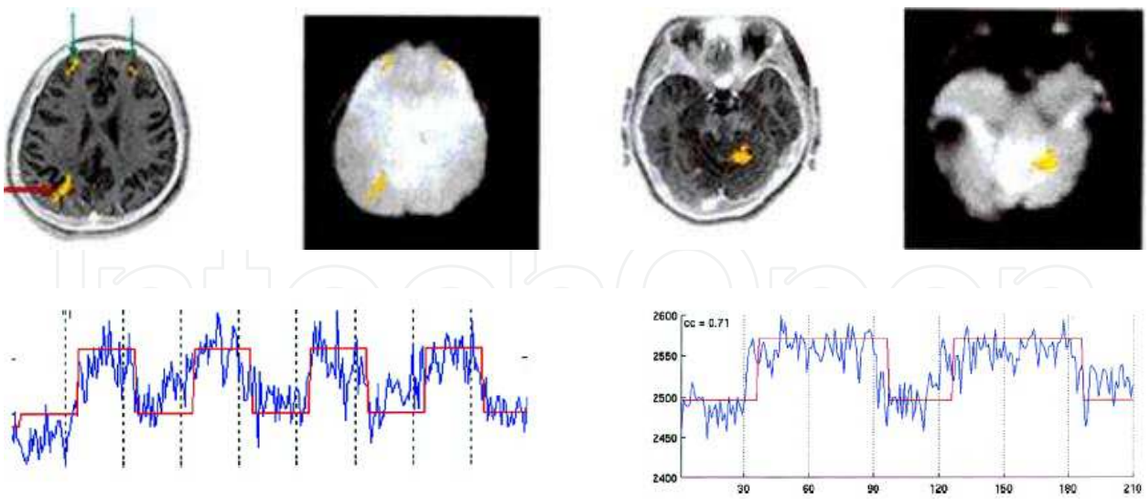

Fig. 12. The figure shows activation in the right intrapareital sulcus of cerebrum cortex lobes (as arrow). The raw image fMRI image did not show ghost or susceptibility effect to cause fictitious activation. After segmentation and processing, corresponding time series of activated pixels showed intensity changes. These intensity changes correlated with boxcar type paradigm. The frontal lobes showed fictitous activation while right intraparietal area showed valid activation map.

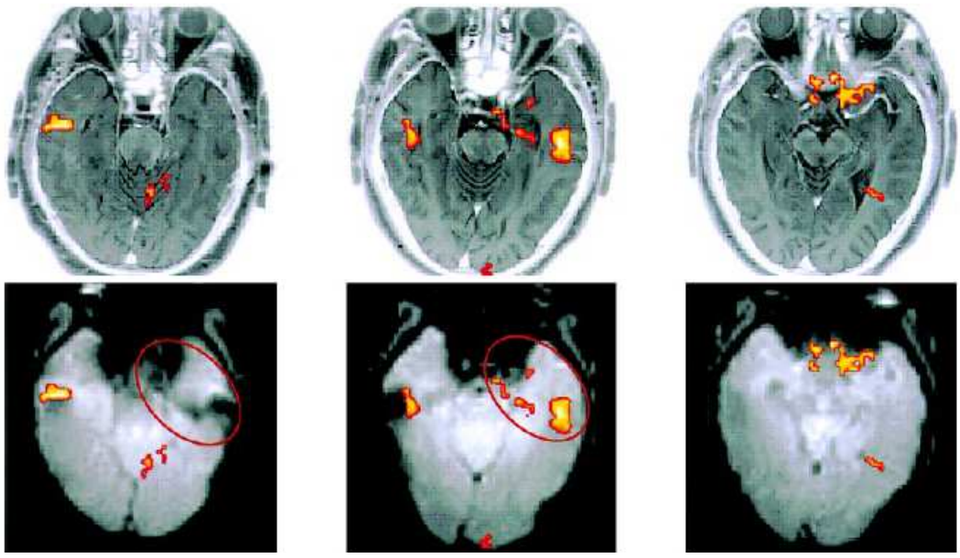

Fig. 13. The figure shows activation in the left cerebellum cortex lobes (as arrow). The raw image fMRI image did not show ghost or susceptibility effect to cause fictitious activation. After segmentation and processing, corresponding time series of activated pixels showed intensity changes. These intensity changes correlated with boxcar type paradigm. The left area showed fictitious activation map due to eye movement.

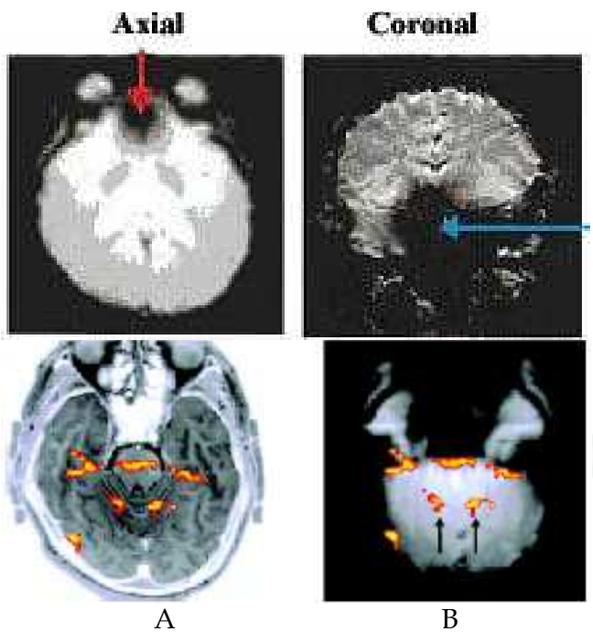

Fig. 14. (On left)The figure shows strong susceptibility effects in axial slice. Note the effect of partial presence of air sinus caused significant distortion in EPI image (arrow in left panel). In coronal slice, air sinus occupied larger image volume (arrow in right panel). (On right) A. activation map on structural (T2R) image. B. Activation EPI image. Emperical or fictitious activation occurred adjacent to structures with strong susceptibility (air sinuses and air cells) True activations sites caused by bilateral hand motion(see arrows in B) get affected by susceptibility on T_2* images.

segmentation and processing, corresponding time series of activated pixels showed intensity changes. These intensity changes correlated with boxcar type paradigm. The frontal lobes showed fictitous activation while right intraparietal area showed valid activation map.

6. Image processing principles

Image processing is the computation process to extract out or sort out important data from large set of image data. To perform extraction and analysis of brain activation locations or Talairach maps, we describe two basic segmentation and registration methods for fMRI image processing and their applications.

6.1 Segmentation

The segmentation task in fMRI is performed by recognition and distinguishing brain areas that respond to a given task or stimulus with high specificity and sensitivity. Two methods 'Bayesian approach' and 'General Linear Model' are common for computation of statistical parameter maps (SPM). The detection of brain activation due to an input stimulus is segmented by statistically comparing images acquired during stimulation (ON state) and those acquired when brain is at rest (OFF state). The results of comparison are expressed by test statistics for each brain voxel in terms of 'likelihood' or 'significant activation' of voxel by the stimulus. Whole brain voxels' likelihood generates SPM map. SPM is an image in which image intensity values represent statistics obtained under null hypothesis of no activation and conform to a certain probability distribution.

'Thresholding' technique using SPM at a significant value can detect brain activation and spatial correlation using 'Gaussian random fields' (GRF) for multivariate Gaussian distribution. This GRF performs the spatial filtering of functional images to minimize pseudo-active brain regions. Alternatively, binary 'Markov random fields' (MRF) models for activation patterns suggested the intensity distribution of SPMs and Bayesian modeling of fMRI time-series inferred the hidden psychological states in fMRI experiments using 'likelihoods' of activation probabilities from these SPMs as shown in Figure 15.

6.1.1 Bayesian approach

A functional brain image is a spatio-temporal signal from brain serial scans taken over time. The posterior probability (Gaussian conditional covariance $\eta_{\theta/y}$, where ($p(\theta/y)$ is proportional to the obtained data depending on times of prior probability of θ as: $p(\theta/y) \alpha p(y/\theta)\, p(\theta)$. The Guass-Markov estimator may be presented as:

$$\eta_{\theta/y} = (X^T C_\varepsilon^{-1} X)^{-1}(X^T C_\varepsilon - 1y) \quad (6)$$

First, preprocessing of images is done and then detection of brain activation analysis is performed [56]. For it, the set of brain voxels is identified from image domain, and the brain scans are corrected for baseline intensity variation and person's head motion. In next step, derivation of SPMs and their statistical analysis by GLM, detects regions of significant activation.

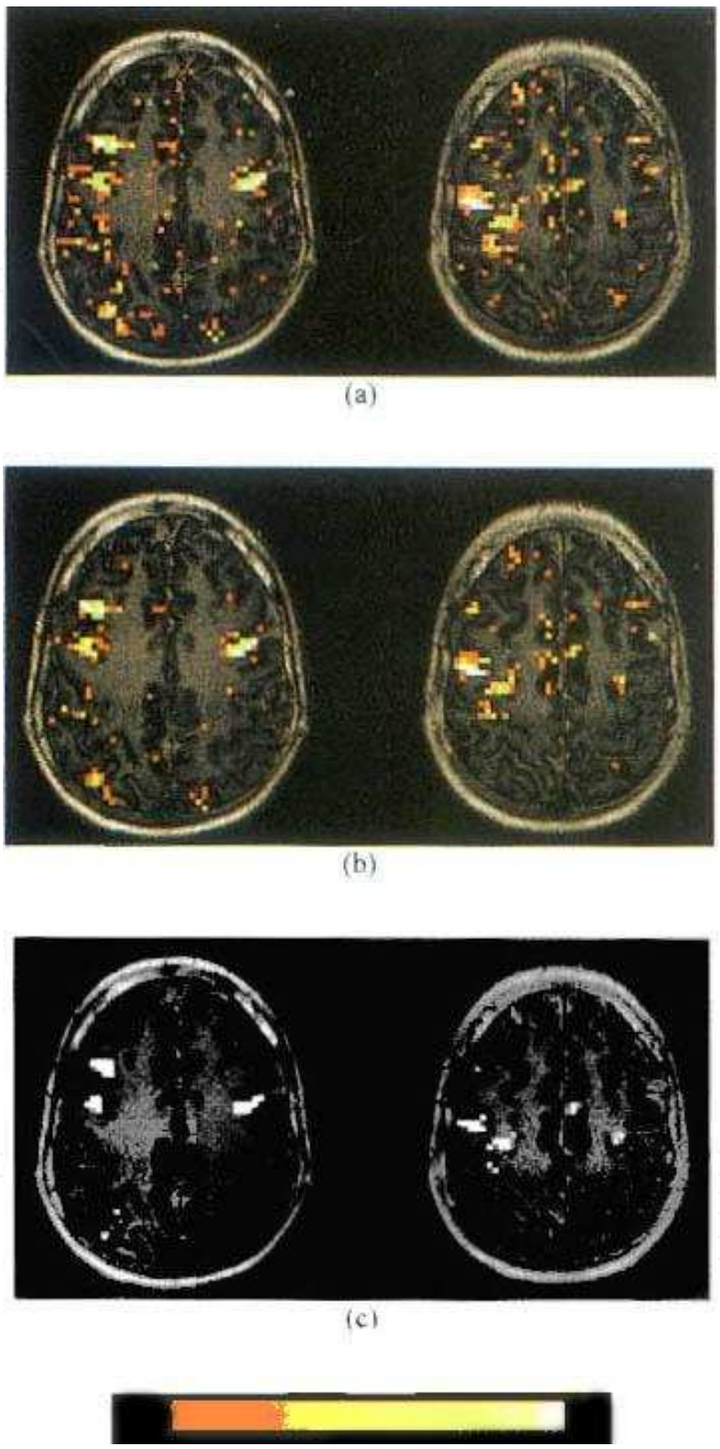

Fig. 15. Activation obtained on two axial brain slices of a representative volunteer in the memory retrieval task by (a) thresholding the SPM{z} at a significant P value = 0.01, (b) using the SPM approach on the SPM{z} with a minimum blob size of three voxels and a significance threshold z = 3.5, and (c) using the MRF approach on the SPM{z}. The significance values (z-values) of the activated voxels are shown color-coded.

6.1.2 F contrasts

Event-related conditions for motor responses are interpreted as hemodynamic response function (HRF) to generate SPM 't' maps as shown in Figure 9. Using design matrix X_o for 'right motor response' regressors look for variance of residuals. The 'F' test computes the sum of squares of "right hand regressors" as following:

$$F df_1, df_2 = \frac{[Y^T(1-P_{xo})Y - Y_T(I-P_x)Y]/\nu_1}{[Y^T(1-P_{xo})Y/\nu_2} \quad (7)$$

with $\nu_1 = tr[(R_o - R)\Sigma_i]$ and $\nu_2 = tr(R\,\Sigma_i)$; $df_1 = tr\,[R_o - R)\,\Sigma_i\,(R_o - R)\,\Sigma_i / tr(R_o - R)\,\Sigma_i]_2$ and $df_2 = tr\,[R\,\Sigma_i\,R\,\Sigma_i / tr(R\,\Sigma_i]_2$

where R_o is projector onto residual space of x_o, and P_x is orthogonal projector onto X. The 'F' contrasts are one-dimensional, in which case 'F' statistics is simply the square of the corresponding 't' statistics. In SPM interface, 'F' contrasts are displayed as images and 't' statistics is displayed as bars [Cao et al. 1999;Rajapakse et al. 2001].

6.1.3 General linear model

Consider an fMRI experiment involving multiple-input stimuli. Let y(t) and $x_o(t)$ denote the values of the fMRI time-series reponse and the input stimulus 'o' at time t, respectively. Let $X_o = (X_o(t);\ t \in \theta)^T$ and the design matrix of experiment by $[X_1X_2....X_n\ x_{n+1}....x_{n+m}]$ where X_1, $X_2....X_n$ represent n stimulus covariates and X_{n+m} represent 'm' dummy covariates such as age, gender etc. If $y = (y(t):\ t \in \theta)^T$ represents the fMRI time-series, the GLM can be written as $y = X_{\beta + \eta}$, $\beta = (\beta_1, \beta_2, ..\beta_{n+m})^T$ denotes the regression coefficients relating the input covariates to the fMRI response, the matrix $X = [H_1X_1\ H_2X_2\ ...H_nX_n\ X_{n+1}.....X_{n+m}]$ represent the design matrix having covariates modified with the modulation matrices $H_o = \{h^k_{ij}\}_{n.m}$ and the components of noise factor η will correlate and distribute normally. The multiplication of 'input' stimulus with 'modulation matrix' both auto-correlate the dispersion in fMRI response. The 'F' statistics estimates the significance of stimulus to generate time-series 'y' and least square estimate of regression coefficients 'β'. Using time-series at voxel site and stimulus condition X_o, the F_o (statistical score) = $\{F_o(p):\ p \in \theta\}$ represents 'F' statistical maps for stimulus 'o' and denoted by SPM $[F_o]$. SPM obtained using one statistics can be converted to another statistics using their grand mean scaling, regressors by parametric modulation, high-resolution basic functions and serial covariance matrix to get cumulative distributions in each voxel. The applications of these smooth and filtered SPM intensity profiles indicate spatial extents of the activated blobs [Rajapakse et al. 2001].

6.1.4 Markov Random Field (MRF) model

This approach presumes that brain activation patterns form MRF to incorporate contextual information. Let us assume that set $a_o = \{a_o(p):p \in \theta\}$ denote a segmentation of an SPM or a configuration of brain activation, where $a_o(p)$ denotes the state of the brain voxel at site p and $a_o(p) = 0$ if the voxel is inactive and $a_o(p) = 1$ if the voxel is activated by the stimulus 'o'. Here a_o represents MRF or activation pattern [Rajapakse et al. 2001]. As the brain voxel is either activated or inactive, the MRF is assumed as binary logistic model. For this contextual

information, preprocessed images find height threshold for smooth statistical map to detect and distinguish activated areas by using 'Euler Characteristics', Benferroni Correction and contextual clustering algorithm [Cao et al. 1999; Rajapakse et al. 2001]. The Euler characteristics E [EC] is:

$$E[EC] = R(4 \log_e 2)(2\pi)^{-3/2} Z_t e^{-1/2} Z_t^2 \quad (8)$$

Where Z-score thresholds between 0–5, R is number of resels. The later is based on the fact that SPM voxel is adjusted with neighborhood information, if differs from expected non-activation value more than a specified decision value. The 'contextual clustering algorithm' estimates cluster parameter, calculates probability distribution and estimates modulation function to classify the voxel as the 'activation' class, otherwise 'nonactivation' class. However, three algorithms viz. 'voxel-wise thresholding', 'cluster-size thresholding' and 'contextual-clustering' have been described earlier [Rajapakse et al. 2001]. Contextual clustering detects activations in small areas with high probability and voxel-wise specificity. 'Benferroni Correction' is based on probability rules and used for calculating family-wise error (FEW) rates P^{fwe} for fMRI as $P^{fwe} = 1 - (1 - \alpha)^n$ where α is single-voxel probability threshold.

6.1.5 Computation of a statistical parametric map

For the purpose of this segmentation, SPM in the voxel i is represented as:

$$SPM\{F_x\}=\{F_k(p): p \in \Omega_B\} \quad (9)$$

Where F statistical map of $F_k(p)$ for stimulus k represents F statistical score and indicates significance of predicting time-series of voxel site p. For image data, first spatial low-pass filtration increases signal-to-noise ratio and sensitivity then $SPM\{F_x\}$ is computed [Rajapakse et al. 2001].

6.1.6 Applied segmentation methods

Voxel-wise thresholding (VWTH) segmentation method of an SPM applies thresholding to each voxel separately. The voxel at location I is considered as active if and only if $z_i < T$ where T is threshold. Cluster-size thresholding (CSTH) explains the cluster 'c' as active if and only if for all voxels within the cluster $z_i < T$ and the size of cluster 'c' is at least 'T' size voxels. Other common use 'contextual clustering algorithm' (CC) was described in steps [Cao et al. 1999;Rajapakse et al. 2001] as:

1. Label the voxels with zi <T as active and other voxels as non-active. Voxels outside the image volume are considered as non-active.
2. Compute for all voxels I the number of active neighbor voxels u_i.
3. Relabel the voxels for which

$$Z_i + \beta/T\,(u_i - N/2) < T \quad (10)$$

Equation 10 represents voxels as active and other voxels as non-active. The number of neighbor voxels equals to 26-connectivity N = 26. The parameter determines the weighing of the contextual information and is usually positive.

4. If the current labeling is same as the labeling in the previous cycle before that, then stop iterations, otherwise return to step 2.

Probability of observing false activation voxels in a whole volume compares the sensitivity of methods by algorithm applied to different data parameter values. The decision parameter value is chosen that gives false activation in approximately 5 % images and 5 % measured false activation voxels.

6.1.7 Sensitivity, segmentation accuracy and robustness

Generally averaged 500 SPMs achieved by different segmentation methods give mean image probability at voxel-level. The less number of false classified voxels as 'active' in the neighborhood of activation represents segmentation accuracy. Noise evaluation by segmentation of different data determines the robustness against spatial autocorrelations. Low robustness is high probability of false activation detection more than the expected probability. To minimize the false detection of activation, registration algorithms are used to perform 3D geometric matching.

6.2 Registration

6.2.1 Basics

Image registration estimates the mapping between a pair of images. Registration performs for each 3D volume with display of movement parameters in continually updating graph to get matching criteria. Combination of 2D shearing operations and Fourier transform based shifting generate accurate high-speed 2D MR image rotation based on factorization of a general 2D planar rotation matrix. 3D arbitrary orthogonal matrix can be factored in to 3D rotations to accomplish 3D image rotation from nine 2D shears. Other approach of linear-in-frequency phase shift in frequency domain applied to 1D fast Fourier transforms (FFTs) generated the image rotation with polynomial interpolation methods [Cox et al.1999; Sarkissian et al. 2003; Ciulla et al.2002].

However, 3D real time image registration (rotation) algorithm chose the axes ordering that resulted in the least intermediate image distortion (minimum net rotation) at proper flip angle about x, y or z-axes i.e. generalized and windowed sinc interpolation. It applied real-time functional MRI acquisition and activation analysis modules within AFNI package. Functional MRI requires the rigid body transformations: small rotations, translations, zooms, rotating tensors and shears in 1–2 degrees or 1–2 voxel dimensions [Cox et al. 1999;Ciulla et al. 2002]. So, repeated linearization of weighted least squares penalty functions with respect to motion parameters accomplishes the registration of a base image to a target image. This method minimized the regional influences and intrinsic variability in functionally active voxels in the brain. However, fMRI registration suffers from motion-related artifacts: interpolation errors, spin excitation in slice, spatial distortion by Gy and Nyquist ghosts. Intensity based intermodal registration AIR use variance of intensity ratios (VIR) cost function. Real-time image reconstruction was reported using Vision 3.5 software in communication with AFNI or TCP/IP sockets for intra- or intercomputer communications. These registration and rotation algorithms are available as AFNI registration and Visualization program [Cox et al. 1999; Nichols et al.2004].

6.3 Post-processing methods for fMRI images

Several post-processing programs 'BrainVoyager', 'AFNI', 'LOFA', 'AIR' etc (read the directory of fMRI softwares in preface) are available as a highly optimized and user-friendly software systems for the analysis and visualization of functional magnetic resonance imaging data [Gokcay et al.1999; Gold et al.1998; Vemuri et al.2003; Friston et al.2002]. These combine surface-based and volume-based tools to study the structure and function of the brain to explore the secrets of the active brain by fast and highly optimized 2D and 3D image analysis and visualization routines, as shown in Figure 16. These are built-in-support for major standard and advanced data formats.

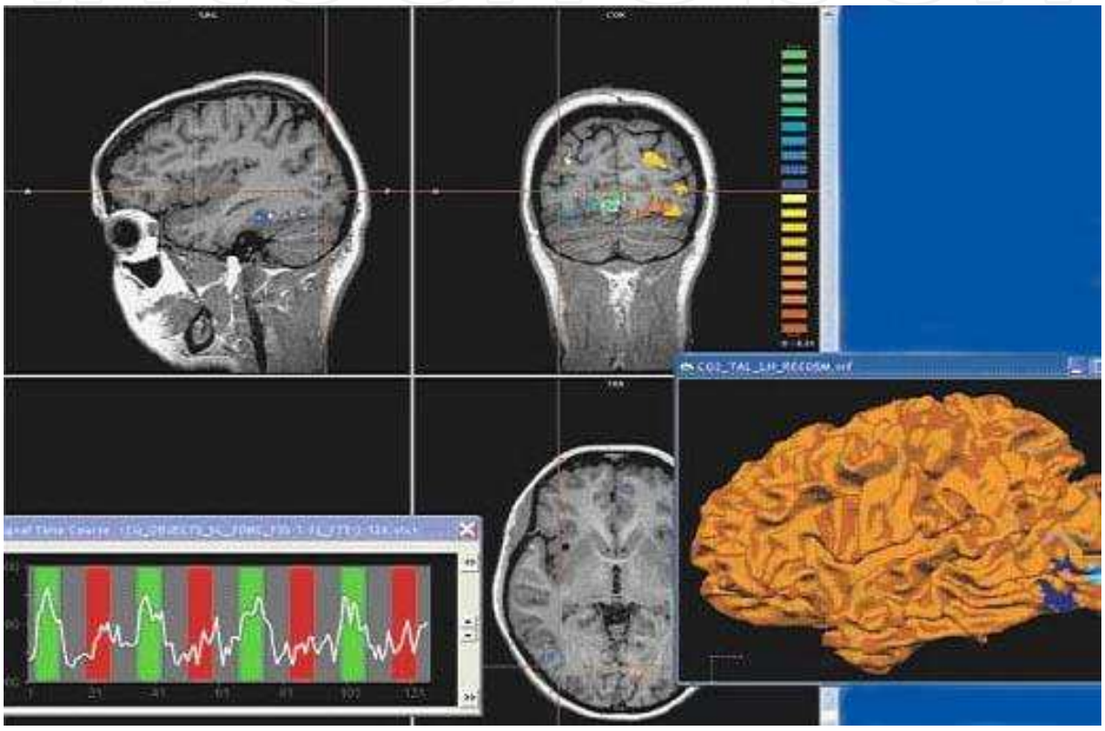

Fig. 16. BrainVoyager is a highly optimized and user-friendly software system for the analysis and visualization of functional and anatomical magnetic resonance imaging data. It combines surface-based and volume-based tools to study the structure and function of the primate brain.

In general, post-processing is completed in following steps:

6.4 Volume-based statistical analysis

Methods include conjunction and Random Effects Analysis (RFX) for single and group analysis via Summary Statistics as following:

1. Fit the model for each subject using different GLMs for each subject or by using a multiple subject GLM.
2. Define the effect of interest for each subject with the contrast factor. Each produces a contrast image containing the contrast of the parameter estimates at each voxel.

3. Feed the contrast images into a GLM that implements a one-sample t test.

The RFX analysis is good technique for making inference from representative subjects [Moutoussis et al.2004]. In fMRI, block analysis, event-related easy selection of regions-of-interest, display of time courses, integration of volume and surface rendering are powerful tools for creation of high-quality figures and movies.

6.5 Advanced methods for automatic brain image-processing

The post-processing offers a comprehensive set of analysis and visualization tools that start its operation on raw data (2D structural and functional matrices) and produces visualization of the obtained results. Now a day, all advanced software features are available via a 'intuitive Windows interface'. Several approaches were performed for surface reconstruction, cortex inflation and flattening; cortex-based statistical data analysis (cbGLM) and inter-subject alignment based on gyral / sulcal pattern; cortex based Independent Component Analysis (cbICA); creation and visualization of EEG / MEG multiple dipole models (fMRI "seeding"); multi-processor support, for ultimate performance; open architecture via COM interface, including scripting and automation [Hong et al. 1999; Kin et al. 2003; Schmitt et al. 2004; Henson et al. 2001].

6.6 Data analysis

It includes data analysis (motion correction, Gaussian spatial and temporal data smoothing, and linear-trend removal, filtering in the frequency domain), correlation analysis, and determination of Talairach coordinates, volume rendering, surface rendering and cortex flattening [Moutoussis et al.2004]. Statistical maps may be computed either in the 2D or 3D representation since structural as well as functional 4D data (space × time) is transformed into Talairach space (see Figures 10 and 11). Talairach transformation is performed in two steps. The first step consists of rotating the 3D data set for each subject to be aligned with the stereotaxic axes. For this step, the locations of the anterior commissure (AC) and the posterior commissure (PC) as well as two rotation parameters for midsagittal alignment have to be specified interactively. In the second step, the extreme points of the cerebrum are specified. These points together with the AC and PC coordinates are then used to scale the 3D data sets into the dimensions of the standard brain of the Talairach and Tournaux atlas [Moutoussis et al.2004]. Isolating the brain gray matter and white matter tissues using region-growing methods, filter operations and the application of 3D templates performs segmentation. Segmentation explores a 3D volume with superimposed pseudocolor-coded statistical maps in a four-window representation showing a sagittal, coronal, transversal and oblique section. Based on a (segmented) 3D data set, a 3D reconstruction of the subjects' head and brain can be calculated and displayed from any specified viewpoint using volume or surface rendering. Parametric and non-parametric statistical maps may be computed and superimposed both on the original functional scans as well as onto T1-weighted 2D or 3D anatomical reference scans. Nonparametric-permutatation approaches are alternate options at low degree of freedom (small sample size to determine intersubject variability) for noisy statistic images when random fields are conservative i.e. smooth variances [Moutoussis et al.2004].

6.7 Volume rendering

It is performed with a fast 'Ray-Casting algorithm'. Lightning calculations are based on 'Phong-shading'. Surface rendering of reconstructed surfaces was performed using OpenGL [Hong et al. 1999].

6.8 The surface reconstruction

The surface reconstruction starts with a sphere (recursively tessellated icosahedron) or a rectangle, which slowly wraps around a (segmented) volume data set. Blood oxygenation level-dependent (BOLD)-based fMRI was performed in the visual cortex, and the foci of fMRI activation utilized as seeding points for 3D fiber reconstruction algorithms, thus provided the map of the axonal circuitry underlying visual information processing [Kim et al. 2003]. A reconstructed cortical surface may be inflated; cut interactively and slowly unfolded minimizing area distortions. Statistical 3D maps may be superimposed on reconstructed, inflated or flattened cortex. Signal time courses may be invoked by simply pointing to any region of a visualized surface.

7. Present knowledge and advances in fMRI data analysis

In last two decades, fMRI technique was improved for fast data acquisition by motion and susceptibility insensitive T_2* weighted EPI, FSE sequences, new task paradigms, motor or sensory task related fMRI robust automated data analysis of brain activation in x, y, and z coordinates as function of time to map out Talairach spaces. SPM data analysis software was developed for matching Talairach coordinates with morphological MRI features. Recent advances in fMRI research in visual and motor events response are extensively reported mainly to identify localized cortical regions by robust image processing segmentation and registration methods, statistical analysis and better spatial resolution using multimodal approaches (fMRI combined with MR spectroscopy, diffusion-weighted imaging, MRI/PET as reviewed in following section. Conventionally, fMRI serves as surface topography patterns related with cognition brain functionality but now art is growing as multimodal fMRI with its adjuncts in characterizing focal or localized region analysis associated with neurological lesions to rule out if focal lesions can affect brain functionalities in various brain areas such as multiple sclerosis lesions, hippocampus size in Alzheimer's Disease, epilepsy as examples. In following sections, we describe advantages of growing imaging technology at high-magnetic field and new possibilities of multimodal imaging.

7.1 High-field MR scanner system is an advantage in fMRI

For high-field fMRI imaging at 3T-11.7T MRI scanners, paramagnetic susceptibility of spin may be related with gyromagnetic ratio (γ) and represented by the Brillouin equation as:

$$\text{Paramagnetic susceptibility} = \frac{h\gamma}{2B_o}\tanh\left[\frac{\left|h\gamma B_o\right|}{\left|2kT\right|}\right] \tag{11}$$

where k is the Boltzmann constant and T absolute temperature.

Susceptibility effect in fMRI increases exponentially as the hyperbolic tangent associated with an increase in the main field, B_o, of the system. T2* detectable activation (ΔI) is significantly increased as shown in Figure 17. Simultaneously, artifacts inducing perturbations also increase. High-field MRI imager system generates T2* contrast for analysis of complex behavioral tasks. It is performed by Independent component-component cross correlation sequence epoch (ICS) as shown in Figure 18. Single subject Ideographic analysis was reported at 3 T systems to locate face-exemplar by regional cortical flat-mapping [Schmitt et al. 2004]. For clinical purposes, 1.5 T systems work well. For advanced neuroimaging investigation, higher field MR systems are essential.

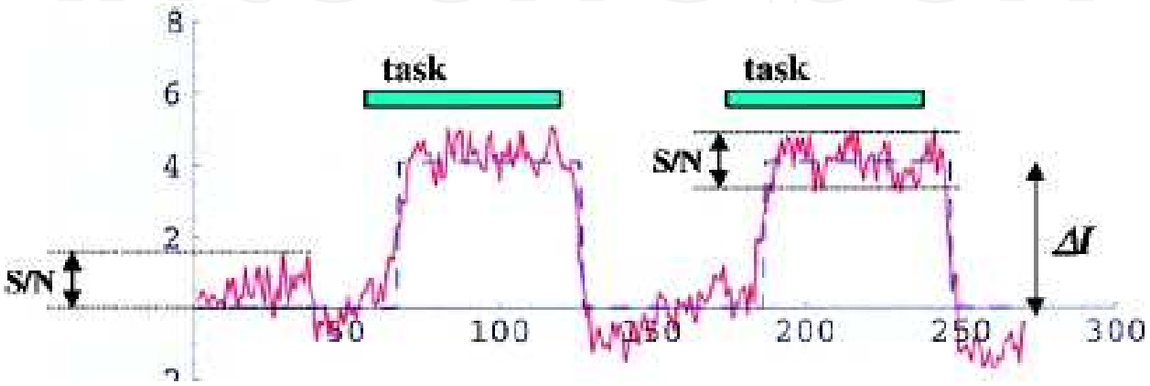

Fig. 17. A typical time series of an activated pixel in primary cortex is shown to represent the performance of horizontal 3T system optimized for fMRI. S/N indicated variation of EPI images, while ΔI, activation induced increase in signal intensity. This time series represents signals from a single voxel volume of 3 mm × 3 mm × 5 mm. The red curves represent raw data and boxcar type model functions shown in blue color.

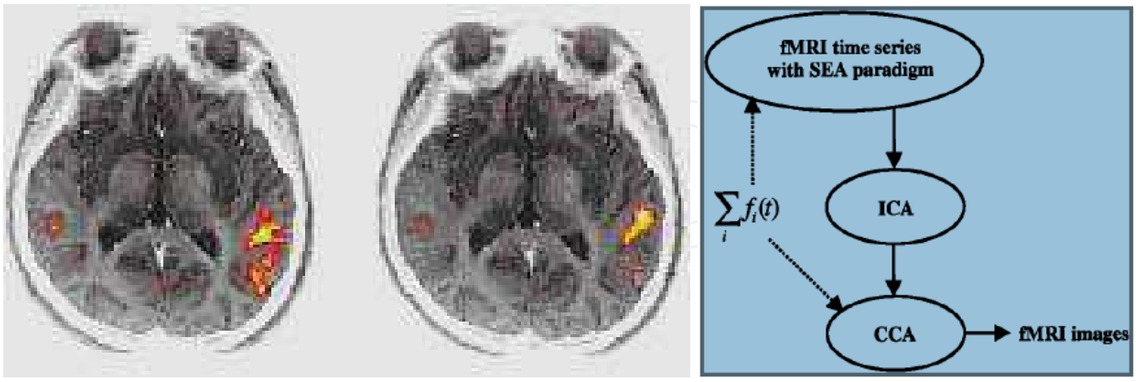

Fig. 18. (On left) Figure represents functional maps shown for comprehension tasks: for reading task (eft panel) and hearing task (right panel). Paradigms requiring tasks of different modalities (visual vs auditory) may provide almost identical activation maps based on the identical abstract concept of "comprehension". Using high field fMRI may provide high quality activation maps to distinguish these activation maps. (On right) Figure shows the Independent component-component cross correlation sequence epoch (ICS).

7.2 fMRI time series analysis

In fMRI, 'time series analysis' by SPM99 is recently used for autocorrection and smoothening. For it, generalized linear model can be expressed as a function of discrete time series, y(t) as:

$$Y(t) = x_c(t)\beta_c + \varepsilon(t) \quad (12)$$

where $x_c(t)$ and $\varepsilon(t)$ are function of time, β_c are time-invariant parameters. Linear time invariance distinguishes neural activity (event) and post-stimulation (epoch) onsets. In general, the resolution of delta function, dt = Tr/T sec and the number of columns = N_c = $N_iN_jN_kN_b$ represent invariance in design matrix. High pass filtering of 'time series' frequency components y(t) get Fourier transformed to remove noise and convolution. Temporal autocorrection in fMRI series is done by 'temporal smoothing' and 'intrinsic autocorrelation' and estimated by 'Auto-Regression' or '1/ f low-pass smoothing' methods to remove bias [Henson et al. 2001].

SPM99 offers 'finite impulse response' (FIR) sets for increased neural activity increases BOLD response 'amplitude' over few seconds based on BOLD from different brain regions such as V1, S1, A1 and higher cortical regions with different vasculature 'Temporal Basis Functions'. FIR sets consist of N_k contiguous box-car functions of peristimulus time, each of duration TH/N_k. TH is maximum duration of high-pass filter. The Fourier set consists of sine Ns and cosine functions of harmonic periods TH, TH/2...TH/N_s. Linear combination of FIR, Fourier sets captures any shape of response in timescale TH/N_k or N_s/TH respectively [Rugg et al. 2002]. 'Event-related Response' and 'Basis sets' were chosen based on stimulus variability and canonical 'Hemodynamic Response Function' and 'F' contrasts determine contribution of different basis sets. Single event- Multi-event type design minimizes the 'contrast error'. Deterministic, static and dynamic stochastic designs use minimum 'stimulus onset synchrony' (SOA_m) and probability of event (for single event design) or transition matrix (for multi-event design) to induce variance over a range of frequencies. Extended softwares are VoxBo, IBASPM, SPM2/5/8,MRIcro, and FSL for better data analysis.

Linear Transform model interprets fMRI signals, origin of the fMRI signals and compares fMRI with neuronal signals. Left and right lateralization for motor cortex stimulation generated visual flash motor response indicative of relationship between different measures of neuronal activity such as single-and multi-unit spiking activity, LFP etc. and reflected neuronal functions. Recently, fMRI signal measured the signal induced by the inputs to a cortical area [Meyer et al.2003].

7.3 Independent component-cross correlation-sequential epoch (ICS) analysis: Image processing

The fMRI acquisition time is usually less per paradigm. For multiple task-oriented studies, analysis of complex higher brain functions is based on the 'principle of functional independence' and functional distinct areas (chronoarchitecture). Independent component-cross correlation-sequential epoch (ICS) segregates distinct areas in cerebral and temporal chronoarchitectonic maps. The different exposures of the brain to natural conditions for different 'durations' segregate the different brain areas for their temporal differences. One subset of natural conditions, reflect free-viewing activity of visual, parietal, temporal areas. However, frontal, pre-frontal cortices functional subdivisions or multivariate paradigms were recently illustrated as shown in Figure 19. A sequential epoch paradigm is composed

to embed the function which correlates to the target multiple behavioral hypothesis **(Σifi(t)).** The simplest function is a 'boxcar function' as employed in many fMRI studies. For it, fMRI time series are subjected to blind separation into independent components by independent component analysis. Subsequently, cross correlation analysis is performed utilizing each embedded function, **f(t)**, as model function to achieve multiple fMRI images as behavioral correlates given by the selected function as an activation map. For the hemodynamic reference function (HRF) following a single sensory stimulation, the time course function represents as model function and ICS becomes a reliable method for event-related fMRI. ICS is useful for event related high-field fMRI where T2* contrast enhances the magnitude of activation than that performed on conventional 1.5 T clinical systems [Kiviniemi et al.2004].

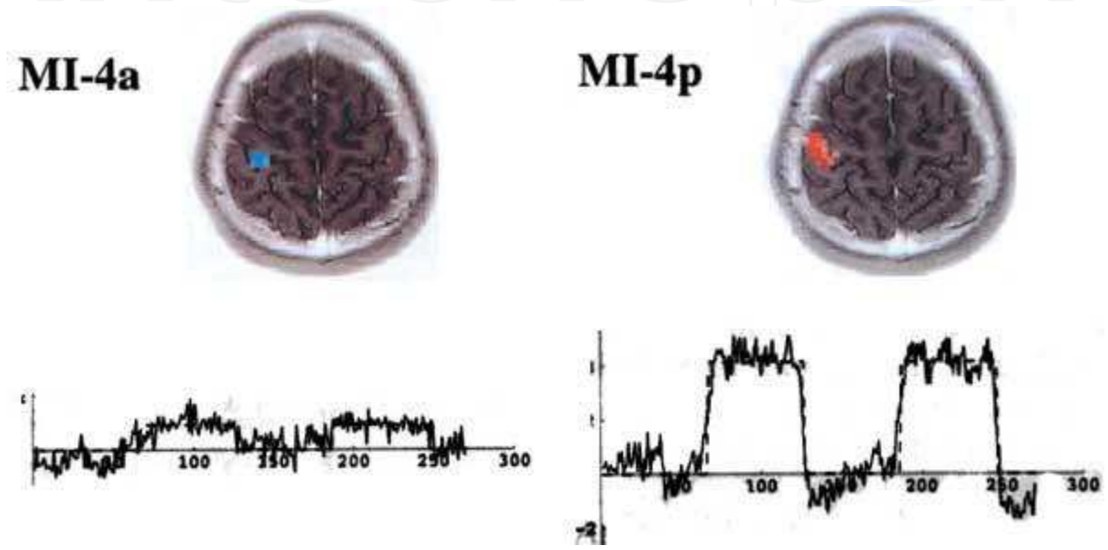

Fig. 19. An example of multivariate analysis in primary motor cortex is represented for revealing the presence of dual representations of constructed multivariate paradigms (MI 4a and MI 4p) in human.

7.4 Brain functional areas

Brain is a complex neural structure as illustrated in Figure 3. Different stimuli affect specific neural activities with result of specific local neuroactivation in brain such as visual, event related, auditory and other motor sensory stimuli cause fMRI visible activation of specific locations in frontal, parietal and temporal lobe regions. We review some of these well-established reports of stimuli in following description.

7.5 Visual stimuli and fMRI activation patterns

- Visual stimuli and event related neural activity by fMRI and image processing methods are reviewed significantly in recent years [18]. Visual areas are recently identified as the boundaries of visual areas V1, V2, V3, V3A, V4, MT/V5, and TEO/V4A in visual cortex and their distribution within the occipital lobe. Motor related areas are known as M1. These corresponding areas are: Broadmann's area (BA 4), SMA (BA 6) and premotor area (BA 6). These fMRI visible areas as shown in Figure 19, are important to interpret fMRI stimulation and its location [Mandeville et al. 1999; Brewer et al.2002]. Recently, new

understanding of quantitative visual field eccentricity function measurements on visual field maps by fMRI were made in macaque visual cortex visual areas. fMRI estimated the average receptive field sizes of neurons in each of several striate and extrastriate visual areas of the human cerebral cortex. Retinotopic mapping procedures determined the boundaries of the visual areas and visualized on flattened occipital cortex, primary visual cortex V1, V2, V3/VP and V3A and V4. In all these areas, receptive fields increased in size with increasing stimulus eccentricity similar to macaque monkeys [Schoenfeld et al.2002]. fMRI maps and the visual area maps represent the distribution of cortical signals and computational homologies between human and monkey. Neural activity and the creation of a new memory trace were observed using functional magnetic resonance imaging (fMRI). Event-related fMRI demonstrated the activity in prefrontal and medial temporal lobe areas associated with successful memory storage. Contrast activity was associated with encoding success and encoding effort using a cue in the form of a letter (R or F). These recent studies suggested the prefrontal activation strongly associated with intentional verbal encoding and left medial temporal activation for successful memory on the subsequent test. Cortical regions sensitive to motion processing receive their inputs only via the primary visual cortex (striate cortex).

- Recently, fMRI evidenced higher-order motion-processing in primates and humans with damaged primary visual cortex (e.g., "blindsight" for motion in the blind visual hemifield) for the existence of a direct thalamic functional pathway exists to extrastriate visual cortical motion processing areas that bypasses primary visual cortex [Schoenfeld et al.2002]. Highfield fMRI retinotopic method was reported to map the neural substrate of retinal slip compensation during visual jitter in flattened cortical format. A novel illusion (visual jitter) suggested the compensation mechanism based on retinal motion. fMRI suggested the pathway from V1 to MT+ involved in the compensation stage in stabilizing the visual world [Sasaki et al.2002]. fMRI demonstrated the sensitivity changes controlled within the visual pathway for responses in human visual area V1 to a constant-amplitude, contrast reversing probe presented on a range of mean backgrounds. fMRI signals from probes initiated in the L and M or S cones. Psychophysical tests showed changes in V1 fMRI cortical BOLD signals by 'mean-field adaptation model' within cone photoreceptor classes [Wade et al.2002]. A new mechanism of hypercapnia and hypocapnia was described as alveolar oxygen and CO_2 gases flux and their effect on BOLD response to visual stimulation. At high magnetic field 7 T, the BOLD signal magnitude and dynamics of hemodynamic response represented the effect of CBF under conditions: hypocapnia, normocapnia, and hypercapnia [Cohen et al.2002].
- Binocular interactions present checkerboard stimuli occurring when subjects view dichoptically. A flickering radial checkerboard stimulation of eyes in binocular or monocular conditions, generate specific responses in striate and extrastriate visual cortex on T2*-weighted images of visual cortex acquired with gradient-echo, echoplanar imaging. The striate area, calcarine fissure BOLD response differed for these stimulation conditions [Buchert et al.2002]. Recently, a neuron location by color-selective mapping method has attracted to compare the relationships of ocular dominance and orientation with responses to high-contrast luminance stimulus and patchy distribution of color selectivity to locate different functional subdivisions of striate cortex in macaque. These color patches with the cytochrome-oxidase (CO) blobs speculated the ocular dominance (OD) column. For it, "Ice cube" model of color-selective regions predicted the organization of orientation and ocular dominance functional hypercolumns in V1

[Landisman et al.2002]. Dipole locations in cortical brain (regional visualization) is developed as a new art by fMRI activations. Neural generators of the visual evoked potential (VEP) generate isoluminant checkerboard stimuli. Using Multichannel scalp recordings, retinotopic mapping and dipole modeling techniques estimated the dipole locations of the cortical regions giving rise to C1, P1, and N1 components of VEP [Di Russo et al.2002]. These locations could be matched to both MRI-visible anatomical brain regions and fMRI activations. Several locations are broadly identified as C1 component (striate cortex; area 17), early phase of the P1 component (dorsal extrastriate cortex of the middle occipital gyrus), late phase of the P1 component (ventral extrastriate cortex of the fusiform gyrus), posterior N 150, anterior N 155 (parietal lobe) in relation to visual-perceptual processes. In other development for complex cognitive tasks, neuronal encoding and fMRI processing strategies segregate retention and retrieval phases of visual short-term memory for objects, places and conjunctions in humans. These tasks were associated with spatio-temporal activation of parietal and prefrontal areas during the retention phase and posterior-anterior and right-left dissociation for spatial versus non-spatial memory [Munk et al.2002].

- The 'perceptual switch' stimulus induces responses in areas calcarine to parieto-occipital and ventral and lateral temporo-occipital cortex to anterior insula. During vection, early motion-sensitive visual areas and vestibular parieto-insular cortex deactivate, whereas higher-order parieto- and temporo-occipital areas respond to optical flow retained identical activity levels. Recent fMRI study showed that these areas displayed transient activations as response to the type of visual motion stimulus and perceptual biostability [Kleinschmidt et al.2002]. fMRI distinguished different neural substrates as 'visual object recognition' sites i.e. lateral occipital and posterior inferior temporal cortex with lower activity for repetitions of both real and non-sense objects; fusiform and left inferior frontal regions with lower activity for repetitions of only real 3D objects; left inferior frontal cortex for different exemplars evidencing dissociable subsystems in ventral visual cortex with distinct view-dependent and view-invariant object representations. Repetition-priming method was proposed for visual stimuli recurring at unpredictable intervals, either with the same appearance or with changes in size, viewpoint or exemplar [Vuilleumier et al.2002].

7.6 Event related potentials and fMRI activation patterns

- Combining event-related potentials (ERP) and fMRI activation provide temporal and spatial resolution, functional connectivity of neural processes of same neural networks within the bilateral occipital gyrus, lingual gyrus; precuneus and middle frontal gyrus; and the left inferior and superior parietal lobe; middle and superior temporal gyrus; cingulate gyrus, superior frontal gyrus and precentral gyrus. It evidenced the correlation within the common activity and time-range in a complex visual language task [Jackson et al.2004]. These tasks comprise specific stimulus-response associations and activate a variety of non-specific cortical regions [Maclin et al.2001]. Dystonia, a movement disorder involves involuntary coordination of agonist and antagonist muscles, which cause abnormal posture or twisting. Event related fMRI technique revealed impairment of muscle contraction and relaxation. Comparison of activated volume in cortical motor areas in dystonia patients with volunteers showed different muscle relaxation and contraction activation volumes as shown in Figure 20. In these tasks, mainly SM1 and SMA activated areas were reduced contra- laterally in dystonia patients as evidenced by time course of fMRI signal in SMA activation area [Oga et al.2002].

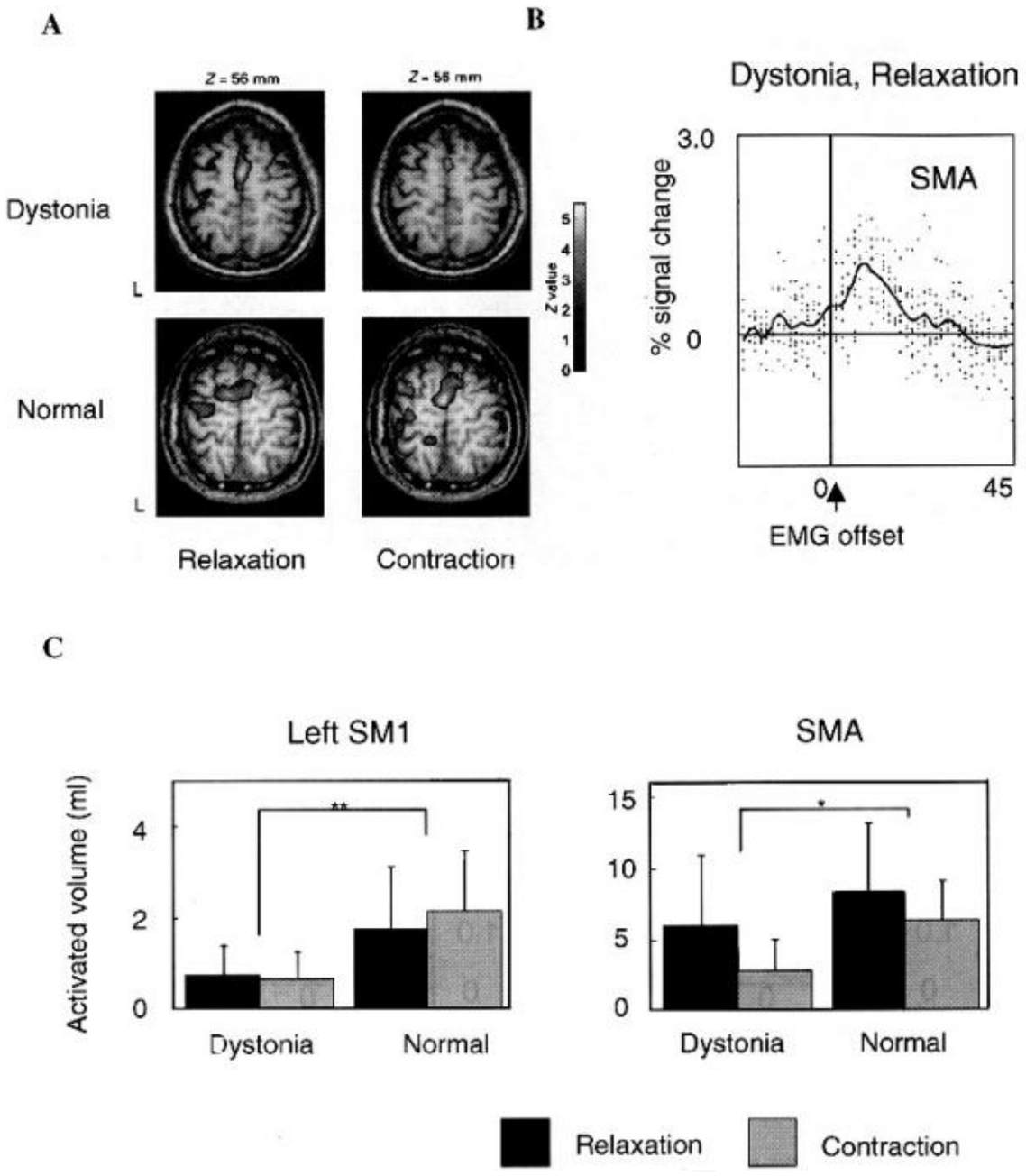

Fig. 20. Figure represents the application of event-related fMRI to dystonia. Comparison of activated volume in motor cortical areas in a patient with dystonia and a normal subject is represented in the muscle relaxation and contraction task. In both tasks, the activated areas in the M1 and SMA were smaller for dystonia while in normal these activated areas were larger (see top 4 panels shown as A). A solid line indicates a mean signal change across ten trials shown as dots. The transient signal change timelocked to EMG offset was observable even in single trial (see panel B). Group data from eight patients and twelve healthy volunteers; demonstrate that activated volumes in the contralateral SM1 and SMA are greater in the healthy volunteers than in the dystonic patients.

7.7 Sensory and motor systems

- Sensory and motor systems interact in complex ways. Voluntary movements with visual attention yield distinct fMRI hemodynamic signals and brain activations i.e. making repetitive finger movements, attending to the color of a visual stimulus or simultaneous finger movement and visual attention. In these processes, the primary motor cortex, supplementary motor area, cerebellum, sparse cerebral cortical and substantial bilateral cerebellar locations get active. Activation-related interactions in the left superior parietal lobule, the right fusiform gyrus, and left insula, recently were indicated their role in visual attention and movement [Indovina et al.2001].
- Different psychological tests have been developed to evaluate frontal tasks of macaque monkeys and humans. Wisconsin Card Sorting Test (WCST) characterized the frontal lobe lesions in macaque monkeys and humans based on behavioral flexibility in the form of cognitive set shifting. Equivalent visual stimuli and task sequence showed transient activation related to cognitive set shifting in focal regions of prefrontal cortex in both monkeys and humans. These functional homologs were located in cytoarchitectonically equivalent regions in the posterior part of ventrolateral prefrontal cortex. This comparative imaging provided insights into the evolution of cognition in primates [Nakahara et al.2002].
- Test-retest precision of functional magnetic resonance imaging (fMRI) by student 't' mapping (STM) is recently described for independent component analysis (ICA) using two or three iterations of visual and auditory stimuli for fMRI scans. Concurrence ratios of the activated voxels divided by the average number of voxels activated in each repetition showed similar test-retest precision of ICA as STM [Nybakken et al.2002].

7.8 High spatial resolution fMRI

High spatial resolution in fMRI showed as dependent on hyperoxic hemodynamic response to neural activity in short duration and it was used to investigate the columnar architecture of ocular dominance within the primary visual cortex [Yoo et al.2004]. For intensity-based non-rigid registration of medical images was developed for atlas based segmentation and intensity-based geometric correction of functional magnetic resonance imaging (fMRI) images by 'Adaptive bases algorithm' to register the smallest structures in the image [Rohde et al.2003].

8. Present developments and future perspectives on fMRI and adjunct imaging multimodal techniques

The goal of this chapter was to introduce the neurophysiological factors and image processing principles of fMRI to suggest potential future applications in neuroscience and physiology. These future directions include neurosurgical planning and improved assessment of risk for individual patients, improved assessment and strategies for the treatment of chronic pain, improved seizure localization, and improved understanding of the physiology of neurological disorders. We look ahead to newer algorithms, enhanced fMRI sensitivity and spatial resolution by use of high field systems, ASL and phase array coils or newer contrast agents [Ugurbil et al.2002]. Presently, other emerging applications of

EEG/MEG, PET and neuropsychological testing along with fMRI are coming up as the benefits of this fMRI technology incorporated into current neuroscience and future patient care. These adjunct methods are:

8.1 Diffusion based functional MRI

Neuronal activity produces some immediate physical changes in cell shape that can be detected because they affect the compartment shape and size for water diffusion. A much improved spatial and temporal resolution for fMRI data collection has now been achieved by using diffusion MRI methodology that can detect these changes in neurons. The abrupt onset of increased neuron cell size occurs before the metabolic response commences, is shorter in duration and does not extend significantly beyond the area of the actual cell population involved. This technique is a diffusion weighted technique (DWI). There is some evidence that similar changes in axonal volume in white matter may accompany activity and this has been observed using a DTI (diffusion tensor imaging) technique. The future importance of diffusion-based functional techniques relative to BOLD techniques is not yet clear.

8.2 Contrast MR

An injected contrast agent such as an iron oxide that has been coated by a sugar or starch (to hide from the body's defense system), causes a local disturbance in the magnetic field that is measurable by the MRI scanner. The signals associated with these kinds of contrast agents are proportional to the cerebral blood volume. While this semi-invasive method presents a considerable disadvantage in terms of studying brain function in normal subjects, it enables far greater detection sensitivity than BOLD signal, which may increase the viability of fMRI in clinical populations. Other methods of investigating blood volume that do not require an injection are a subject of current research, although no alternative technique in theory can match the high sensitivity provided by injection of contrast agent.

8.3 Arterial spin labeling

Arterial Spin Labelling (ASL), also known as arterial spin tagging, is an MRI technique capable of measuring cerebral blood flow (CBF) *in vivo*. ASL is capable of providing cerebral perfusion maps, without requiring the administration of a contrast agent or the use of ionising radiation, as it uses magnetically-labelled endogenous blood water as a freely-diffusible tracer. It was first proposed in 1992 and has since benefited from a number of modifications aimed at improving its robustness. ASL can monitor changes in CBF with activation and fMRI studies can therefore be conducted using ASL instead of relying on the BOLD effect. ASL fMRI is less popular than BOLD, as it suffers from a lower signal to noise ratio, can be less sensitive to weak stimuli and its temporal resolution is poorer than in BOLD studies. On the plus side, it can provide quantitative measures of a single well-defined parameter, CBF, whose baseline value can also be determined in the same experiment. It has also been found to outperform BOLD in terms of stability to slow signal drifts and localization of the activation area. The ASL activation signal is believed to be dominated by changes in the capillary bed of the activated area of

the cortex, wheareas the BOLD signal is likely to be dominated by changes in the oxygenation of nearby veins.

8.4 Magnetic resonance spectroscopic imaging

Magnetic resonance spectroscopic imaging (MRS) is another, NMR-based process for assessing function within the living brain. MRS takes advantage of the fact that protons (hydrogen atoms) residing in differing chemical environments depending upon the molecule they inhabit (H_2O vs. protein, for example) possess slightly different resonant properties (chemical shift). For a given volume of brain (typically > 1 cubic cm), the distribution of these H resonances can be displayed as a spectrum.

The area under the peak for each resonance provides a quantitative measure of the relative abundance of that compound. The largest peak is composed of H_2O. However, there are also discernible peaks for choline, creatine, N-acetylaspartate (NAA) and lactate. Fortuitously, NAA is mostly inactive within the neuron, serving as a precursor to glutamate and as storage for acetyl groups (to be used in fatty acid synthesis) — but its relative levels are a reasonable approximation of neuronal integrity and functional status. Brain diseases (schizophrenia, stroke, certain tumors, multiple sclerosis) can be characterized by the regional alteration in NAA levels when compared to healthy subjects. Creatine is used as a relative control value since its levels remain fairly constant, while choline and lactate levels have been used to evaluate brain tumors.

8.5 Diffusion tensor imaging

Diffusion tensor imaging (DTI) is a related use of MR to measure anatomical connectivity between areas. Although it is not strictly a functional imaging technique because it does not measure dynamic changes in brain function, the measures of inter-area connectivity it provides are complementary to images of cortical function provided by BOLD fMRI. White matter bundles carry functional information between brain regions. The diffusion of water molecules is hindered across the axes of these bundles, such that measurements of water diffusion can reveal information about the location of large white matter pathways[Awojoyogbe et al. 2011]. Illnesses that disrupt the normal organization or integrity of cerebral white matter (such as multiple sclerosis) have a quantitative impact on DTI measures.

8.6 fMRI and EEG

Functional MRI has high spatial resolution but relatively poor temporal resolution (of the order of several seconds). Electroencephalography (EEG) directly measures the brain's electrical activity, giving high temporal resolution (~milliseconds) but low spatial resolution. The two techniques are therefore complementary and may be used simultaneously to record brain activity.

Recording an EEG signal inside an MRI system is technically challenging. The MRI system introduces artifacts into the EEG recording by inducing currents in the EEG leads via Faraday induction. This can happen through several different mechanisms. An imaging sequence applies a series of short radiofrequency pulses which induce a signal in the EEG

system. The pulses are short and relatively infrequent, so interference may be avoided by blanking (switching off) the EEG system during their transmission. Magnetic field gradients used during imaging also induce a signal, which is harder to remove as it is in a similar frequency range to the EEG signal. Current is also induced when EEG leads move inside the magnet bore (i.e. when the patient moves during the exam). Finally, pulsed blood flow in the patient in the static magnetic field also induces a signal (called a ballistocardiographic artifact), which is also within the frequency range of interest. The EEG system also affects the MRI scan. Metal in the EEG leads and electrodes can introduce susceptibility artifacts into MR images. Care must also be taken to limit currents induced in the EEG leads via the MRI RF system, which could heat the leads sufficiently to burn the subject. Having simultaneously recorded EEG and fMRI data, the final hurdle is to co-register the two datasets, as each is reconstructed using a different algorithm, subject to different distortions in EEG-fMRI.

In recent years, lot of future excitement is evident in the following areas of brain information extraction by segmentation and registration methods applied to fMRI and above-mentioned multimodal adjunct methods. These include mainly automated nonlinear labeling; and automated surface reconstructions. Automated surface reconstruction appears to be possible by: i. cortical surface-based analysis by segmentation and surface reconstruction [Fischl et al.1999a]; ii. cortical surface-based analysis by inflation, flattening, and a surface-based coordinate system [Fischl et al.1999b]. Automated anatomical brain labeling may be performed by: i. whole brain segmentation: automated labeling of neuro-anatomical structures in the human brain [Fischl et al.2002]; ii. multipatient registration of brain fMRI using intensity and geometric features [Cachier et al.2001]; iii. automatic detection and labeling of the human cortical fields in magnetic resonance data sets [Lohmann et al.1998]. With advancement of neurophysiological principles, more and more facts are explored on physiological origin of neuroactivation and brain functional relationships. Recently a biophysical mechanism of low-frequency drift in blood-oxygen-level-dependent (BOLD) functional magnetic resonance imaging (fMRI) (0.00-0.01 Hz) was reported by exploring its spatial distribution, dependence on imaging parameters, and relationship with task-induced brain activation. Authors showed that the spatial distribution of low-frequency drifts in human brain followed a tissue-specific pattern, with greater drift magnitude in the gray matter than in white matter. In gray matter, the dependence of drift magnitudes on TE was similar to that of task-induced BOLD signal changes, i.e., the absolute drift magnitude reached the maximum when TE approached T(2)* whereas relative drift magnitude increased linearly with TE. By systematically varying the flip angle, it was found that drift magnitudes possessed a positive dependence on image intensity. In fMRI studies with visual stimulation, a strong positive correlation between drift effects at baseline and task-induced BOLD signal changes was observed both across subjects and across activated pixels within individual participants. Unique point was that intrinsic, physiological drift effects are a major component of the spontaneous fluctuations of BOLD fMRI signal within the frequency range of 0.0-0.1 Hz[Yan et al.2009]. A rare attempt was made to integrate complementary functional and structural MRI data in a patient with localization-related epilepsy with partial and secondarily generalized seizures and a hemiparesis due to a malformation of cortical development (MCD) in the right hemisphere by using EEG-triggered functional MRI (fMRI), diffusion tensor imaging (DTI), and chemical shift imaging

(CSI). fMRI revealed significant changes in regional blood oxygenation associated with interictal epileptiform discharges within the MCD. DTI showed a heterogeneous microstructure of the MCD with reduced fractional anisotropy, a high mean diffusivity, and displacement of myelinated tracts. CSI demonstrated low N-acetyl aspartate (NAA) concentrations in parts of the MCD. MR methods described functional, microstructural, biochemical characteristics of the epileptogenic tissue and pathophysiology of epilepsy [Bauewig et al.2001]. Recent focus of fMRI research is shifting towards integrated neurofunctional data acquisition such as electrophysiology (EEG), with simultaneous neurochemical mapping and diffusion tensor/molecular perfusion [Horwitz et al.2002; McDonald et al.2010; Matsumoto et al.2005; Vartiainen et al.2011]. However, success is awaited because of non-localized nature of diffusion tensor and fMRI sensitive brain functionality, wide variation in neurochemical changes in the same brain regions. In case of such possibility of integrated data acquisition, multimodal approaches such as fMRI/MRS/PET will be single step feasible one platform imaging method available in clinical neuroimaging in near future [Dale et al.2001]. The basis of imaging is Munro-Kellie doctrine principle to predict decline in cerebral venous blood volume secondary to an increase in cerebral arterial blood volume in fMRI identical to image blood flow by H_2O^{15}-PET [Fox et al.1984].

8.7 Multimodal methods of fMRI combined with adjuncts in localized neurodegeneration

The art of multimodal imaging approach is based on the fact that single platform can be used in one step imaging by using fMRI, EEG, diffusion MRI, MRS, PET, simultaneously in selected area of brain[Awojoyogbe et al. 2011]. Some notable examples are illustrated below.

Multiple Sclerosis: First author reported measurement of neurochemicals in growing MS lesions with MRSI. Gamma-aminobutyric Acid (GABA) was used as indicator of brain functionality [Sharma 2004; Sharma 2002]. Several reports indicated the value of fMRI as multimodal method combined with DTI, MRS, PET to assess cognitive impairment in multiple sclerosis. Such approach was based on the link between structural, metabolic and functional changes in multiple sclerosis [Filippi et al.2001]. It was interesting that neurochemicals and cognitive impairment in MS showed significant role [Tartaglia et al.2006]. This approach was further extended in other study based on the fact that cognitive impairment by fMRI was related with structural MRI changes and metabolic changes by PET [Sorensen et al.2006]. Overall, growing art of fMRI is now established in multiple sclerosis [Korsholm et al.2007]. Other investigators reported the lesions as a result of inflammatory demyelination which led to fMRI visible cognitive impairment [Rachbauer et al.2006]. Since the development of fMRI based multimodal imaging in evaluation of lesions, main obstacle remained coregistration and statistical data analysis [Fu et al.1996]. Now robust techniques of fMRI data analysis are available for structural and functional MRI correlation analysis to make evaluation of cortical reorganization in MS. We illustrate one example of T2*-weighted echo planar images acquired (64 · 64 matrix over a 24-cm field of view). These consisted of 25 consecutive, 4-mm thick axial sections, with TR/TE (repetition time/echo time) = 3000/50 ms, a 90_ flip angle and one excitation. [Peresedova et al.2009; Rocca et al.2009]. Motor task paradigm (‘stop’ and ‘start’) acoustic signals for hand motion

was used for fMRI1 and 2 acquisition and voxel Z score analysis in x,y,z coordinates to make Talairach space by linear transformation as shown in Table 1.

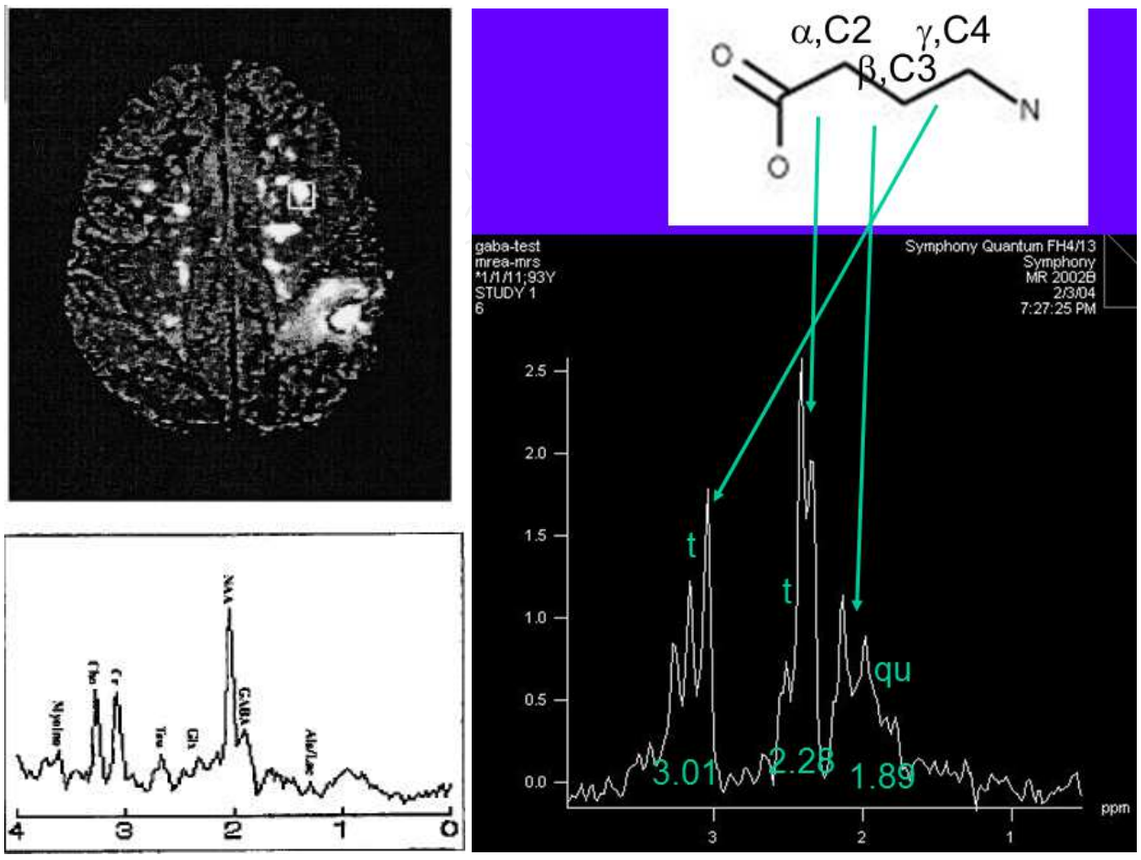

Fig. 21. A typical MS lesion rich voxel (upper panel) with respective spectral peaks is shown (panel at bottom), showing peak at 1.85 ppm for GABA metabolites (see enlarged panel on left at bottom and right) in 48 year old female patient. For simplicity, metabolites are labeled for lipids at 0.8-1.2 ppm, lactate-alanine at 1.2-1.33 ppm, NAA at 2.01 ppm, Cr at 3.0 ppm, Cho at 3.2 ppm, Myo-inositol at 3.6 ppm, Taurine at 2.8 ppm, Gltamine/Glutamate (Glx) , GABA peaks at 1.85, ethanolamine at 3.8 ppm, Glycine at 3.55 ppm, Threonine at 1.31 ppm (see panel on left at bottom). Reproduced with permission of reference Sharma 2004.

Alzheimer's Disease is a diffused injury due to neurofibrillary amyloid plaque formation affecting cortical and posterior cingulate region with fMRI visible cognitive impairment. Recently, multimodal imaging was established and reviewed to assess cognitive impairment using magnetic resonance spectroscopy, perfusion, and diffusion tensor properties [Zimmy et al.2011; Minati et al.2007]. However, other biophysical properties such as changes in biomagnetic, electrophysiological signals along with metabolite screening were established as link between neurochemical and magnetic interactions in brain during development of Alzheimer's Disease [Maesti et al.2005]. In quest of measuring these changes, deformable shape-intensity models were reported in Alzheimer's Disease, dementia [Zhu et al.2003; Gilberto et al.1996; Giacometti et al.1994].

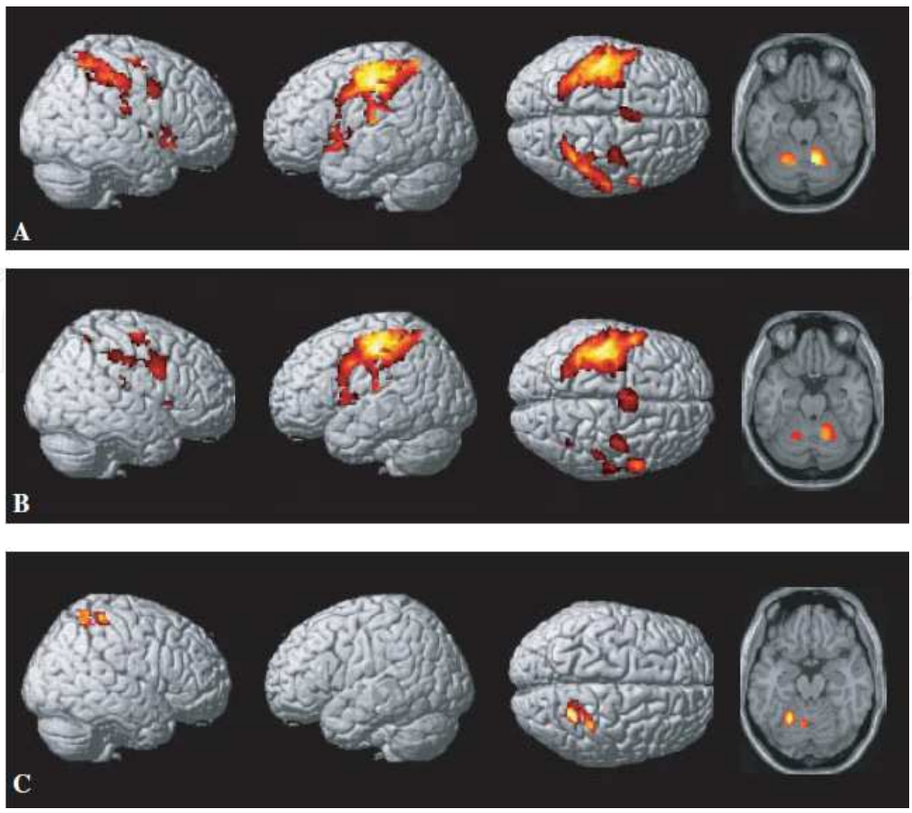

Brain area	Baseline		Follow-up	
	Talairach coordinates (x, y, z)	Z	Talairach coordinates (x, y, z)	Z
L sensorimotor cortex (BA 1–4)	-44, -19, 43	5.80	- 38, -19, 47	7.57
L inferior parietal lobule (BA 40)	- 46, -32, 52	5.24	-53, -30, 24	4.15
			-49, -38, 48	3.87
L lateral premotor cortex (BA 6)	-34, -5, -55	5.14	-59, 6, 32	6.69
L supplementary motor area (BA 6)	-2, -1, 55	4.27	-2, 1, 53	5.44
L lentiform nucleus	-12, -12, -1	5.22	-26, 3, 9	5.21
L thalamus	-12, -11,13	4.72	-16, -17, 3	5.09
L insula	-55, 12, 3	4.69	-49, -20, 16	5.65
L cerebellum	-18, -55, -17	5.17	— —	-----
R sensorimotor cortex (BA 1–4)	42, 0, 52	4.06	45, -27, 40	4.55
R inferior parietal lobule (BA 40)	32, -48, 54	5.23	40, -33, 40	4.63
			61, -2, 19	4.39
R lateral premotor cortex (BA 6)	30, -7, 57	5.08	61, 7, 29	5.77
	57, 8, 36	4.81	36, -11, 58	5.26
R superior parietal cortex (BA 7)	32, -48, 54	5.23	36, -52, 56	4.67
R lentiform nucleus	—	—	22, -2, 2	4.37
R thalamus	12, -7, 13	4.17	12, -6, 13	4.17
R insula	57, 19, -4	4.78	57, 16, 1	4.22
	47, 4, -1	3.91		
R cerebellum	18, 55, 17	6.59	18, -53, -18	6.22
Vermis	2, -67, -10	5.89	2, -50, -3	4.68

Z = voxel level.

Fig. 22. Group maps generated from random effect analysis showing (A) task-related activation at fMRI1, (B) task-related activation at fMRI2 and (C) task-related activity

decrease between the two fMRI studies during right hand movement in 18 patients with multiple sclerosis. Significant areas of activation (in colour) are superimposed on 3D brain rendering and slices (z = -18). Areas of decreased activity (fMRI1 > fMRI2) (C) included the right (ipsilateral) sensorimotor cortex and the left (contralateral) cerebellum. One-sample t-test ($P < 0.05$) corrected at the cluster level. Images are displayed according to the neurological convention. Location of significant neuroactivations ($P < 0.05$ corrected at the cluster level) during right hand movement in 18 MS patients are shown in table (see at bottom) at baseline and at follow-up within group analysis (one sample t-test SPM99 using Talairach coordinates in images on top). Reproduced with permission from reference Pantano et al.2005.

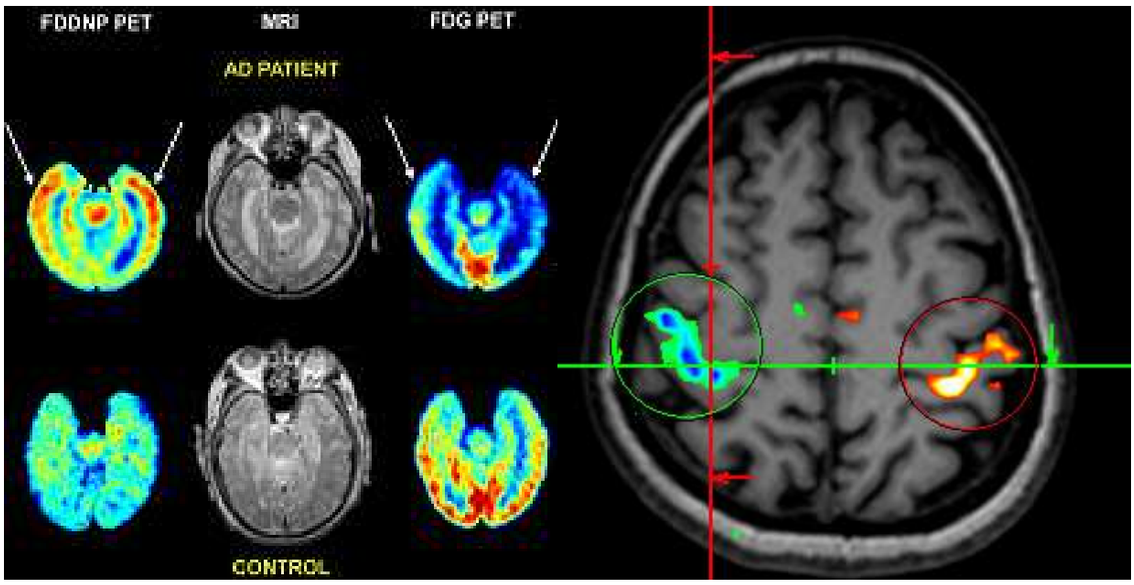

Fig. 23. Multimodal imaging is shown for fMRI combined with FDDNP-PET and FDG-PET to illustrate sites of high oxygen or high glycolysis metabolism (on left panel) and locations of neuroactivation (on right panel). Copyright material from webpage http://precedings.nature.com/documents/4317/version/1

Initial application of fMRI in epilepsy evaluation was exciting [Sullivan et al.2005]. However, epilepsy is considered as focal brain disease with possible regional changes in brain function, diffusion tensor properties, neurochemicals [Krakow et al.1999]. fMRI with simultaneous neurochemical measurement serves as noninvasive quantitative MR modality to assess the epileptogenic foci [Morales-Chacon 2001]. Diffusion tensor tractography and neurochemicals with fMRI pinpoint the location of motor neuron disease and schizophrenia[Nelles et al.2008; Steel et al.2001]. MRS and DTI methods have been developed to evaluate and assess the cerebral small vessel disease progress and its chemical nature [Nitkunan et al. 2006]. Being more sentive to electrophysiological response epilepsy is best evaluated by electrophysiology and use of electrodes [Guye et al.2002]. Now attempts

were made in the direction of metabolic and oxygen changes during epileptogenic development in cortex using PET/MRI/DTI [Chandra et al.2006].

9. Conclusion

Present chapter introduces the concept of functional MRI and physiological basis of neuroactivation as a result of motor and sensory tasks to make change in blood oxygen and blood flow characteristics in some established neurodegenerative diseases with cognitive impairments in multiple sclerosis, Alzheimer's Disease, epilepsy. fMRI technique is offshoot of structural MRI with other adjunct imaging techniques and it serves as multimodal imaging to map out structural and functional changes in different brain areas simultaneously to decipher the information of neurochemical, anatomical, regional differences to make assessment of cognition impairment, brain recovery and brain functionality before and after disease or drug treatment. Major issues still remain unsolved of wide variability of fMRI sensitive neuroactive locations, fast acquisition, low resolution and rapid data analysis. With available robust and rapid techniques and software, it will be easier to map brain functions simultaneous with neurochemical and metabolic imaging.

10. Disclosure of interest

Authors have no conflict of interest. The chapter is based on the contents from a review article authored by authors of this chapter and cited as reference 108 in the reference list.

11. References

Amunts, K.., Schleicher, A., Ditterich, A., Zilles, K. (2003). Broca's region: Cytoarchitectonic Asymmetry and Developmental Changes. *The Journal of Comparative Neurology,* 465, pp72-89.

Awojoyogbe, O.B., Dada,M. (2011) Basis for the application of analytical models of the Bloch NMR flow equations for functional resonance imaging(fMRI): A review. Renet Patents on Medical Imaging.1,pp 33-67.

Bandettini, P.A., Ungerleider, L.G. (2001) From neuron to BOLD: new connections. Nature Neurosci. 4, pp864–866.

Bandettini, P.A., Cox, R.W. (2000) Event related fMRI contrast when using constant interstimulus interval: Theory and experiment. Magn Reson Med. 30, pp161–173.

Baudewig, J., Bittermann, H.J., Paulus, W., Frahm, J. (2002) Simultaneous EEG and functional MRI of epileptic activity: a case report. Clinical Neurophysiology,112(7), pp1196-1200.

Horwitz B, Poeppel D. How Can EEG/MEG and fMRI/PET Data Be Combined? Human Brain Mapping, 17, pp1–3.

Binkofski, F., Amunts, K., Stephen, K.M., Posse, S., Schormann, T., Freund, H.J., Zilles, K. & Seitz, R.J. (2000). Broca's Region Subserves Imagery of Motion: A Combined Cytoarchitectonic and fMRI Study. *Human Brain Mapping*, 11, pp273-285

Brewer, A.A., Press, W.A., Logothetis N.K., Wandell, B.A. (2002) Visual areas in macaque cortex measured using functional magnetic resonance imaging. J Neurosci. 22, pp10416–26.

Buchert, M., Greenle,e M.W., Rutschmann, R.M., Kraemer, F.M., Luo, F., Hennig, J. (2002) Functional magnetic resonance imaging evidence for binocular interactions in human visual cortex. Exp Brain Res. 145, pp334–9.

Buxton, R.B., Frank, L.R. (1997) A model for the coupling between cerebral blood flow and oxygen metabolism during neuronal stimulation. J Cereb Blood Flow Metab.17, pp 64–72.

Cachier, P., Mangin, J.F., Pennec, X., Riviere, D., Papadopoulos-Orfanos, D., Regis, J., Ayachi, N. (2001) Multipatient registration of brain MRI using intensity and geometric features. In: Niessan W, Vierever M, editor. Proceedings of MICCAI. LNCS 2208. pp. 734–742.

Cao, Y., Vikingstad, E. M., George, P. K., Johnson, A. F., & Welch, K. M. A. (1999). Cortical Language Activation in Stroke Patients Recovering From Aphasia With Functional MRI. *Stroke, 30,* pp. 2331-2340.

Caplan, D., Alpert, N., Waters, G. & Olivieri, A. (2000). Activation of Broca's Area by Syntactic Processing Under Conditions of Concurrent Articulation. *Human Brain Mapping*, 9, pp 65–71.

Chandra PS, Salamon N, Huang J, Wu JY, Koh S, Vinters HV, Mathern GW. FDG-PET/MRI coregistration and diffusion-tensor imaging distinguish epileptogenic tubers and cortex in patients with tuberous sclerosis complex: a preliminary report. Epilepsia. 2006;47(9):1543-9.

Cheng, K., Waggoner, R.A., Tanaka, K.. (2001) Human ocular dominance columns as revealed by high field functional magnetic resonance imaging. Neuron. 32, pp. 359–374.

Ciulla, C., Deek, F.P. (2002) Performance assessment of an algorithm for the alignment of fMRI time series. Brain Topogr. 14, pp. 313–32.

Cohen, E.R., Ugurbil, K., Kim, S.G. (2002) Effect of basal conditions on the magnitude and dynamics of the blood oxygenation level-dependent fMRI response. J Cereb Blood Flow Metab. 22, pp. 1042–53.

Cox, R.W., (1999) Jesmanowicz A. Real-time 3D image registration for functional MRI. Magn Reson Med. 42, pp.1014–1018.

Cox, R.W.(1996) AFNI: software for analysis and visualization of functional magnetic resonance neuroimages. Comput Biomed Res. 29,pp.162–73.

Dale, A.M., Halgren, E. (2001) Spatiotemporal mapping of brain activity by integration of multiple imaging modalities. Curr Opin Neurobiol. 11, 2, pp.202-8.

Di Russo, F., Martinez, A., Sereno,M.I., Pitzalis, S., Hillyard, S.A.(2002) Cortical sources of the early components of the visual evoked potential. Hum Brain Mapp.15, pp. 95–111.

Disbrow, E.A., Slutsky, D.A., Roberts, T.P., Krubitzer, L.A. (2000) Functional MRI at 1.5 Tesla: A comparison of the blood oxygenation level-dependent signal and electrophysiology. Proc Natl Acad Sci USA. 97, pp. 9718–9723.

Fadiga, L. & Craighero, L. (2006a). Hand actions and speech representation in Broca's area. *Cortex*, 42, pp. 486–490

Fadiga, L., Craighero, L., Desto, M. F., Finos, L., Cotillon-Williams, N. et al. (2006b). Language in shadow, *Social Neuroscience*, 1, pp.77–89

Filippi, M.(2001) Linking structural, metabolic and functional changes in multiple sclerosis. Eur J Neurol. 2001 Jul;8(4):291-7.

Fink, G.R., Manjaly, Z.M., Stephen, K.E., Gurd, J.M., Zilles, K., Amunts K., Marshall, J.C. (2006). A Role for Broca's Are Beyond Language Processing: Evidence from Neuropsychology and fMRI. In: *Broca's Region*. Amunts, K. & Grodzinsky, Y. (Eds). Oxford University Press, Oxford

Fischl, B., Sereno, M.I., Dale, A.M. (1999) Cortical Surface-based analysis I: Segmentation and Surface Reconstruction. Neuroimage. 9, pp. 195–207.

Fischl, B., Sereno, M.I., Dale, A.M. (1999) Cortical Surface-based analysis II: Inflation, Flattening, and a Surface-Based Coordinate System. Neuroimge. 9, pp.179–194.

Fischl, B., Salat, D.H., Busa, E., Albert, M., Dieterich, M., Haselgrove, C., van der Kouwe, A., Killiany, R., Kennedy, D., Klaveness, S., Montillo, A., Makris, N., Rosen, B., Dale, A.M. (2002) Whole brain segmentation: Automated labeling of neuroanatomical structures in the human brain. Neurone. 33, pp.341–355.

Fox, P.T., Mintun, M.A., Raichle, M., Herscovitch, P. (1984) A noninvasive approach to quantitative functional brain mapping with H_2O^{15} Positron Emission Tomography. J Cereb Blood Flow Metab, 4, pp.329-333.

Fransson, P., Kruger, G., Merboldt, K.D., Frahm, J. (1997)A comparative FLASH and EPI study of repetitive and sustained visual activation. NMR Biomed. 10, pp.204–7.

Friederici, A. (1998). The neurobiology of language comprehension, In : *Language Comprehension: A Biological Perspective,* Friederici, A.D. (Ed.),Springer, Berlin/Heidelberg/New York, pp. 263-301.

Friston, K.J., Glaser, D.E., Henson, R.N.A., Kiebel, S., Phillips, C., Ashburner, J.(2002) Classical and Bayesian inference in neuroimaging applications. Neuroimage. 16, pp.484–512.

Fu, L., Wolfson, C., Worsley, K.J., De Stefano, N., Collins, D.L., Narayanan S, Arnold, D.L.(1996) Statistics for investigation of multimodal MR imaging data and an application to multiple sclerosis patients. NMR Biomed. 9,8, pp.339-46.

Giacometti, A.R., Davis, P.C., Alazraki, N.P., Malko, J.A. (1994) Anatomic and physiologic imaging of Alzheimer's disease. Clin Geriatr Med.10,2, pp.277-98.

Gilberto González, R. (1996) Molecular and functional magnetic resonance neuroimaging for the study of dementia. Ann N Y Acad Sci. 777, pp.37-48.

Gokcay, D., Mohr, C.M., Crosson, B., Leonard, C.M., Bobholz, J.A. (1999) LOFA: software for individualized localization of functional MRI activity. Neuroimage. 10, pp.749–55.

Gold, S., Christian, B., Arndt, S., Zeien, G., Cizadlo, T., Johnson, D.L., Flaum, M., Andreasen, N.C. (1998) MRI statistical software packages: a comparative analysis. Hum Brain Mapp. 6, pp.73–84.

Goodyear, B.G., Menon, R.S.. (2001) Brief visual stimulation allows mapping of ocular dominance in visual cortex using fMRI. Human Brain Mapp. 14, pp.210–217.

Greewe, T., Bornkessel, I., Zysset, S., Wiese, R., von Cramon, Y.D., Schlesewsky, M. (2005). The Reemergence of the Unmarked: A New Perspective on the Language-Specific Function of Broca's Area. *Human Brain Mapping*, 26, pp.178–190.

Guye, M., Le Fur, Y., Confort-Gouny, S., Ranjeva, J.P., Bartolomei, F., Régis, J, Raybaud, C.A., Chauvel, P., Cozzone, P.J. (2002) Metabolic and electrophysiological alterations in subtypes of temporal lobe epilepsy: a combined proton magnetic resonance spectroscopic imaging and depth electrodes study. Epilepsia. 43,10, pp.1197-209.

Haslinger, B., Erhard, P., Kampfe, N., Boecker, H., Rummeny, E., Schwaiger, M., Conrad, B., Ceballos-Baumann, A.O.(2001) Event related functional magnetic resonance imaging in Perkinson's disease before and after levodopa. Brain. 124, pp.558–570.

Henson, R.N., Rugg, M.D., Friston, K.J. (2001) The choice of basis functions in the eventrelated fMRI. Neuroimage. 15, pp.83–97.

Hickok, G., Poeppel, D.(2007).The cortical organization of speech processing. *Nature Reviews Neuroscience*, 8, pp.393-402

Hong, L., Kaufman, A.E. (1999) Fast Projection-Based Ray-Casting Algorithm for Rendering Curvilinear Volumes. IEEE Trans Visual and Comp Graph. 5, pp.322–332.

Indovina, I., Sanes, J.N. (2001) Combined visual attention and finger movement effects on human brain representations. Exp Brain Res. 140, pp.265–79.

Jackson, G.M., Swainson, R., Mullin, A., Cunnington, R., Jackson, S.R. (2004) ERP correlates of a receptive language-switching task. Q J Exp Psychol A. 57, pp.223–40.

Jueptner, M., Weiller, C. (1995) Does measurement of regional cerebral blood flow reflect synaptic activity: implication for PET and fMRI. Neuroimaging. 2, pp.148–156.

Kiebel, S., Holmes, A., Poline, J.B., Kherif, F., Penny, W. (2004) The general Linear Model; Contrasts and classical inference. In: Frackowiak RSJ, Friston KJ, Frith CD, Dolan RJ, Price CJ, Jeki S, Ashburner J, Penny W, editor. Human Brain Function. Chapters 37 and 38. Elsevier Academic Press, London. pp. 749–779

Kim, D.S., Kim, M., Ronen, I., Formisano, E., Kim, K.H., Ugurbil, K., Mori, S., Goebel R.(2003) In vivo mapping of functional domains and axonal connectivity in cat visual cortex using magnetic resonance imaging. Magn Reson Imaging. 21, pp.1131–40.

Kim, D.S., Duong, T.Q., Kim, S.G. (2003) High resolution mapping of iso-orientation columns by fMRI. Nature Neurosci. 3, pp.164–169.

Kim, S.G., Rostrup, E., Larsson, H.B., Ogawa, S., Paulson, O.B. (1999) Determination of relative CMRO2 from CBF and BOLD changes: Significant increase of oxygen consumption rate during visual stimulation. Magn Reson Med. 41, pp.1152–1161.

Kim, S.G. (1995) Quantification of relative cerebral blood flow change by flowsensitive alternating inversion recovery (FAIR) technique: Application to functional mapping. Magn Reson Med. 34, pp.293–301.

Kim, D.S., Duong, T.Q., Kim, S.G. (2000) High-resolution mapping of iso-orientation columns by fMRI. Nature Neurosci. 3, pp.164–169.

Kiviniemi, V., Kantola, J.H., Jauhiainen, J., Tervonen, O. (2004) Comparison of methods for detecting nondeterministic BOLD fluctuation in fMRI. Magn Reson Imaging. 22, pp.197–203

Kleinschmidt, A., Thilo, K.V., Buchel, C. (2002) Neural correlates of visual-motion perception as object- or self-motion. Neuroimage. 16, pp.873–82.

Korsholm, K., Mathiesen, H.K., Lund, T.E. (2007) Functional magnetic resonance imaging in multiple sclerosis. Ugeskr Laeger. 169,26, pp.2518-20.

Krakow, K., Wieshmann, U.C., Woermann, F.G., Symms, M.R., McLean, M.A., Lemieux, L., Allen, P.J., Barker, G.J., Fish, D.R., Duncan, J.S.(1999) Multimodal MR imaging: functional, diffusion tensor, and chemical shift imaging in a patient with localization-related epilepsy. Epilepsia. 1999;40(10):1459-62.

Kutas, M., Federmeier, K.D., Coulson, S., King, J.W. & Münte, T.F. (2000). Language. In: *Handbook of Psychophysiology*, Cacioppo, J.T., Tassinary, L.G. & Berntson, G. (Eds). Cambridge University Press, Cambridge. pp. 576-601.

Kwong, K.K., Chesler, D.A., Weisskoff, R.M., Donahue, K.M., Davis, T.L., Ostergaard, L., Campbell, T.A., Rosen, B.R. (1995) MR perfusion studies with T1-weighted echo planar imaging. Mag Reson Med. 34, pp.878–887.

Landisman, C.E., Ts'o, D.Y. (2002) Color processing in macaque striate cortex: relationships to ocular dominance, cytochrome oxidase, and orientation. J Neurophysiol. 87, pp.3126–37.

Lee, S.P., Silva, A.C., Ugurbil, K., Kim, S.G. (1999) Diffusion-weighted Spin-echo fMRI at 9.4T: Microvascular/tissue Contribution to BOLD Signal Changes. Magn Reson Med. 42, pp.919–928.

Logothetis, N.K., Pauls, J., Augath, M., Trinath, T., Oeltermann, A. (2001) A neurophysiological investigation of the basis of fMRI signal. Nature. 412, pp.150–157.

Lohmann, G., Yves von Cramon, D. (1998) Automatic detection and labeling of the human cortical fields in magnetic resonance data sets. In: Buckhardt H, Neumann B, editor. In Computer Vision, Fifth European Conference, EECV Friburg, Germany. Springer-Verlag, Berlin, pp. 369–381.

Maclin, E.L., Gratton, G., Fabiani, M. (2001) Visual spatial localization conflict: an fMRI study. Neuroreport. 12, pp.3633–6.

Maess, B., Koelsch, S., Gunter, T., Friederici, A. (2001). Musical syntax is processed in Broca's area: an MEG study. *Nature Neuroscience*, 4, pp.540-545.

Maestú, F., García-Segura, J., Ortiz, T., Montoya, J., Fernández, A., Gil-Gregorio, P., Campo, P., Fernández, S., Viaño, J., Portera, A. (2005) Evidence of biochemical and biomagnetic interactions in Alzheimer's disease: an MEG and MR spectroscopy study. Dement Geriatr Cogn Disord. 20,2-3, pp.145-52.

Mandeville, J.B., Marota, J.J., (1999) Ayata C, Zaharchuk G, Moskowitz MA, Rosen BR, Weisskoff RM. Evidence of a cerebral post-arteriole windlissel with delayed compliance. J Cereb Blood Flow Metab. 19, pp.679–689.

Matsumoto, A., Iidaka, T., Haneda, K., Okada, T., Sadato, N. (2005) Linking semantic priming effect in functional MRI and event-related potentials. Neuroimage. 24,3, pp.624-34.

Mayville, J.M., Bressler, S.L., Fuchs, A., Kelso, J.A. (1999) Spatiotemporal reorganization of electrical activity in the human brain associated with a timing transition in rhythmic auditory-motor coordination. Exp Brain Res. 127, pp.371–381.

McDonald, C.R., Thesen, T., Carlson, C., Blumberg, M., Girard, H.M., Trong,netrpunya, A., Sherfey, J.S., Devinsky, O., Kuzniecky, R., Dolye, W.K., Cash, S.S., Leonard M.K., Hagler, D.J. Jr, Dale, A.M., Halgren, E. (2010)Multimodal imaging of repetition priming: Using fMRI, MEG, and intracranial EEG to reveal spatiotemporal profiles of word processing. Neuroimage. 53,2, pp.707-17.

Meinzer, M., Harnish, S., Conway, T., Crosson, B. (2011) Recent developments in functional and structural imaging of aphasia recovery after stroke. *Aphasiology*, 25,3, pp.271-290.

Meyer, F.G. (2003) Wavelet-based estimation of a semiparametric generalized linear model of fMRI time-series. IEEE Trans Med Imaging. 22, pp.315–22.

Miki, A., Liu, G.T., Englander, S.A., Raz, J., van Erp, T.G., Modestino, E.J., Liu, C.J., Haselgrove, J.C. (2001) Reproducibility of visual activation during checkerboard stimulation in functional magnetic resonance imaging at 4 Tesla. Jpn J Ophthalmol. 45, pp.151–5.

Minati, L., Grisoli, M., Bruzzone, M.G. (2007) MR spectroscopy, functional MRI, and diffusion-tensor imaging in the aging brain: a conceptual review. J Geriatr Psychiatry Neurol. 20,1, pp.3-21.

Morales-Chacón, L. (2001) Magnetic resonance spectroscopy and functional magnetic resonance images: non-invasive alternatives for identifying epileptogenic foci. Rev Neurol. 32,3, pp.234-6.

Moutoussis, K., Zeki, S. (2004) The Chronoarchitecture of the Human Brain: Functional Anatomy Based on Natural Brain Dynamics and the Principle of Functional Independence. In: Frackowiak RSJ, Friston KJ, Frith CD, Dolan RJ, Price CJ, Jeki S, Ashburner J, Penny W, editor. Human Brain Function. Chapter 13. Elsevier Academic Press, London, pp. 201–229.

Müller, H.P., Kassubek, J. (2007) Multimodal Imaging in Neurology: Special Focus on MRI Applications and MEG. Synthesis Lectures on Biomedical Engineering, 2,1, pp.1-75.

Munk, M.H., Linden, D.E., Muckli, L., Lanfermann, H., Zanella, F.E., Singer, W., Goebel, R. (2002) Distributed cortical systems in visual short-term memory revealed byevent-related functional magnetic resonance imaging. Cereb Cortex. 12, pp.866–76.

Nakada, T., Fujii, Y., Kwee, I.L. (2001) Brain strategies for reading in the second language are determined by the first language. Neurosci Res. 40, pp.351–35.

Nakahara, K., Hayashi, T., Konishi, S., Miyashita, Y.(2002) Functional MRI of macaque monkeys performing a cognitive set-shifting task. Science. 295, pp.1532–6.

Nakai, T., Matsuo, K., Kato, C., Okada, T., Moriya, T., Isoda, H., Takehara, Y., Sakahara, H. (2001) BOLD contrast on a 3T magnet: detectibility of the motor areas. J Comput Assit Tomogr. 25, pp.436–445.

Nelles, M., Block, W., Träber, F., Wüllner, U., Schild, H.H., Urbach, H. (2008) Combined 3T diffusion tensor tractography and 1H-MR spectroscopy in motor neuron disease. AJNR Am J Neuroradiol. 29,9, pp.1708-14.

Nichols, T., Holmes, A. (2004) Non parametric permutation tests for functional neuroimaging. In: Frackowiak RSJ, Friston KJ, Frith CD, Dolan RJ, Price CJ, Jeki S,

Ashburner J, Penny W, editor. Human Brain Function Chapters 46. Elsevier Academic Press, London. pp. 887–908.

Nitkunan, A., McIntyre, D.J., Barrick, T.R., O'Sullivan, M., Shen, Y., Clark, C.A., Howe, F.A., Markus, H.S.(2006) Correlations between MRS and DTI in cerebral small vessel disease. NMR Biomed. 19,5, pp.610-6.

Novick, J.M, Trueswell, J.C. & Thompson-Schill, S.L. (2010). Broca's Area and Language Processing: Evidence for the Cognitive Control Connection, *Language and Linguistics Compass,* 4,10, pp.906-924.

Nybakken, G.E., Quigley, M.A., Moritz, C.H. (2002) Test-retest precision of functional magnetic resonance imaging processed with independent component analysis. Neuroradiology. 44, pp.403–6.

Oga, T., Honda, M., Toma, K., Murase, N., Okada, T., Hanakawa, T., Sawamoto, N., Nagamine, T., Konishi, J., Fukuyama, H., Kaji, R., Shibasaki, H. (2002) Abnormal cortical mechanisms of voluntary muscle relxation in patients with writer's cramp: An fMRI study. Brain. 125, pp. 895–903.

Ogawa, S., Menon, R.S., Kim, S.G., Ugurbil, K. (1998) On the characteristics of functional MRI of the brain. Ann Rev Biophy and Biomol Struct. 27, pp.447–74.

Ogawa, S., Lee, T.M., Nayak, A.S., and Glynn, P. (1990). "Oxygenation-sensitive contrast in magnetic resonance image of rodent brain at high magnetic fields". Magnetic Resonance in Medicine 14 , 1, pp.68–78.

Optiz, B., Friederici, A.D. (2007). Neural Basis of Processing Sequential and Hierarchical Syntactic Structures. *Human Brain Mapping*, 28, pp. 585-592.

Pantano, P., Mainero, C., Lenzi, D., Caramia, F., Donenico lannetti, G., Piattella, M.C., Pestalozza, I., Legge, S.D., Bozzao, L., Pozzilli, C. (2005) A longitudinal fMRI study on motor activity in patients with multiple sclerosis. Brain, 128, pp. 2146-2153.

Patel, A. (2003). Language, music, syntax and the brain. *Nature Neuroscience*, 7, pp.674–681

Binkofski, F., Buccino, G. (2004). Motor functions of the Brocas region'. *Brain and Language*, 89, pp.362-369.

Peelen, M.V., Downing, P.E. (2011). The role of occipitotemporal body-selective regions in person perception. *Cognitive Neuroscience*,

Peresedova, A.V., Konovalov, R.N., Krotenkova, M.V., Zavalishin, I.A., Trifonova, O.V.(2009) Cortical reorganization in multiple sclerosis with movement disorders detected by functional MRI (own observations and literature data). Zh Nevrol Psikhiatr Im S S Korsakova. 109,7, Suppl 2, pp.38-43.

Preibisch, C., Haase, A. (1999) Functional MR imaging of the human brain using FLASH: influence of various imaging parameters. J Magn Reson. 140, pp.162–71.

Rachbauer, D., Kronbichler, M., Ropele, S., Enzinger, C., Fazekas, F. (2006) Differences in cerebral activation patterns in idiopathic inflammatory demyelination using the paced visual serial addition task: an fMRI study. J Neurol Sci. 244,1-2, pp.11-6.

Rajapakse, J.C., Priyaratna, J. (2001) Bayesian approach to segmentation of statistical parametric maps. IEEE Trans on Biomed Eng. 48, pp.1186–1194.

Reber, P.J., Siwiec, R.M., Gitleman, D.R., Parrish, T.B., Mesulam, M.M., Paller, K.A.(2002) Neural correlates of successful encoding identified using functional magnetic resonance imaging. J Neurosci. 22, pp.9541–8.

Rocca, M.A., Valsasina, P., Ceccarelli, A., Absinta, M., Ghezzi, A., Riccitelli, G., Pagani, E., Falini, A., Comi, G., Scotti, G., Filippi, M.(2009) Structural and functional MRI correlates of Stroop control in benign MS. Hum Brain Mapp. 30,1, pp.276-90.

Rohde, G.K., Aldroubi, A., Dawant, B.M. (2003)The adaptive bases algorithm for intensity-based nonrigid image registration. IEEE Trans Med Imaging. 22, pp.1470–9.

Rugg, M.D., Henson, R.N. (2002) Episodic memory retrival: an event-related functional neuroimaging perspective. In: Parker AE, Wilding EL and Bussey T, editor. In the Cognitive Neuroscience of Memory Encoding and Retrieval. Psychology Press, Hove. pp. 150–189.

Russ, M.O., Cleff, U., Lanfermann, H., Schalnus, R., Enzensberger, W., Kleinschmidt, A(2002) Functional magnetic resonance imaging in acute unilateral optic neuritis. J Neuroimaging. 12, pp.339–50.

Schmitt, F., Grosu, D., Mohr, C., Purdy, D., Salem, K., Scott, K.T., Stoeckel, B.(2004) 3 Tesla MRI: successful results with higher field strengths. Radiologe. 44, pp.31–47.

Sharma, R., Sharma, A. (2004) Physiological basis and image processing in functional magnetic resonance imaging: Neuronal and motor activity in brain. *BioMedical Engineering OnLine* 3,13 doi:10.1186/1475-925X-3-13

Sharma, R. (2002) Serial Amino-neurochemicals Analysis in Progressive Lesion Analysis of Multiple Sclerosis by Magnetic Resonance Imaging and Proton Magnetic Resonance Spectroscopic Imaging. Magn Reson Med Sci 1,3, pp.169-173.

Shibata, K., Osawa, M., Iwata, M. (2000) Visual evoked potentials in cerebral white matter hyperintensity on MRI. Acta Neurol Scand. 102, pp.230–5.

Singh, M., Kim, S., Kim, T.S. (2003) Correlation between BOLD-fMRI and EEG signal changes in response to visual stimulus frequency in humans. Magn Reson Med. 49, pp.108–14.

Sørensen, P.S., Jønsson, A., Mathiesen, H.K., Blinkenberg, M., Andresen, J., Hanson, L.G., Ravnborg, M. (2006) The relationship between MRI and PET changes and cognitive disturbances in MS. J Neurol Sci. 245,1-2, pp.99-102.

Steel, R.M., Bastin, M.E., McConnell, S., Marshall, I., Cunningham-Owens, D.G., Lawrie, S.M., Johnstone, E.C., Best, J.J. (2001) Diffusion tensor imaging (DTI) and proton magnetic resonance spectroscopy (1H MRS) in schizophrenic subjects and normal controls. Psychiatry Res. 106,3, pp.161-70.

Sarkissian, E., Bowman, K.W. (2003) Application of a nonuniform spectral resampling transform in Fourier-transform spectrometry. Appl Opt. 42, pp.1122–31.

Sasaki, Y., Murakami, I., Cavanagh, P., Tootell, R.H.(2002) Human brain activity during illusory visual jitter as revealed by functional magnetic resonance imaging. Neuron. 35, pp. 1147–56.

Schoenfeld, M.A., Heinze, H.J., Woldorff, M.G. (2002) Unmasking motion-processing activity in human brain area V5/MT+ mediated by pathways that bypass primary visual cortex. Neuroimage. 17, pp.769–79.

Sullivan, J.E. 3rd, Detre, J.A.(2005) Functional magnetic resonance imaging in the treatment of epilepsy. Curr Neurol Neurosci Rep. 5,4, pp.299-306.

Tartaglia, M.C., Arnold, D.L. (2006) The role of MRS and fMRI in multiple sclerosis. Adv Neurol. 98, pp.185-202.

Tegeler, C., Strother, S.C., Anderson, J.R., Kim, S.G. (1999) Reproducibility of BOLD based functional MRI obtained at 4 T. Hum Brain Mapp. 7, pp.267–283.

Thompson-Schill, S.L. (2005). Dissecting the Language Organ: A new Look at the Role of Broca's Area in Language Processing. In: *Twenty-First Century Psycholinguistics. Four Cornerstones*, Cutler A, (Ed.), Lawrence Erlbaum Associates, Mahwah, NJ.pp. 173-190.

Toma, K., Nakai, T. (2002) Functional studies in human motor control studies and clinical applications. Mag Reson Med Sci. 1, pp.109–120.

Turner, R., Jezzard, P., Wen, H., Kwong, K.K., Le Bihan, D., Zeffiro, T., Balaban, R.S.(1993) Functional mapping of the human visual cortex at 4 and 1.5 T using deoxygenation contrast EPI. Mag Reson Med. 29, pp.277–279.

Ugurbil, K. (2002) Magnetic Resonace Studies of Brain Function and Neurochemistry. Annu Rev Biomed Eng. 2, pp.633–60.

Vartiainen, J., Liljeström, M., Koskinen, M., Renvall, H., Salmelin, R.(2011) Functional magnetic resonance imaging blood oxygenation level-dependent signal and magnetoencephalography evoked responses yield different neural functionality in reading. J Neurosci. 31,3, pp.1048-58.

Vemuri, B.C., Ye, J., Chen, Y., Leonard, C.M. (2003) Image registration via level-set motion: applications to atlas-based segmentation. Med Image Anal. 7, pp. 1–20.

Villringer, A. (1999) Physiological changes during brain activation. In: Moonen CTW, Bandenitti PA, editor. In "Functional MRI". Springer-verlag, Berlin; pp. 3–13.

Vuilleumier, P., Henson, R.N., Driver, J., Dolan, R.J.(2002) Multiple levels of visual object constancy revealed by event-related fMRI of repetition priming. Nature Neurosci. 5, pp.491–9.

Wade, A.R., Wandell, B.A. (2002) Chromatic light adaptation measured using functional magnetic resonance imaging. Neurosci. 22, pp. 8148–57.

Yan, L., Zhuo, Y., Ye, Y., Xie, S.X., An, J., Aguirre, G.K., Wang, J.. (2009) Physiological origin of low-frequency drift in blood oxygen level dependent (BOLD) functional magnetic resonance imaging (fMRI) Magnetic Resonance in Medicine. 61,4, pp. 819–827.

Yoo, S.S., Talos, I.F., Golby, A.J., Black, P.M., Panych, L.P. (2004) Evaluating requirements for spatial resolution of fMRI for neurosurgical planning. Hum Brain Mapp. 21, pp.34–43.

Zaharchuk, G., Ledden, P.J., Kwong, K.K., Reese, T.G., Rosen, B.R., Wald, L.L. (1999) Multislice perfusion and perfusion territory imaging in humans with separate label with image coils. Magn Reson Med. 44, pp.92–100.

Zaini, M.R., Strother ,S.C., Anderson, J.R., Liow, J.S., Kjems, U., Tegeler, C., Kim, S.G. (1999) Comparison of matched BOLD and FAIR 4.0T-fMRI with [^{15}O] water PET brain Volumes". MedicalPhysics. 26, pp.1559–1567.

Zhu, X.P., Du, A.T., Jahng, G.H., Soher, B.J., Maudsley, A.A., Weiner, M.W., Schuff, N. (2003) Magnetic resonance spectroscopic imaging reconstruction with deformable shape-intensity models. Magn Reson Med. 50,3, pp. 474-82.

Zimny, A., Szewczyk, P., Trypka, E., Wojtynska, R., Noga, L., Leszek, J., Sasiadek, M.(2011) Multimodal Imaging in Diagnosis of Alzheimer's Disease and Amnestic Mild Cognitive Impairment: Value of Magnetic Resonance Spectroscopy, Perfusion, and Diffusion Tensor Imaging of the Posterior Cingulate Region. J Alzheimers Dis. PMID:21841260

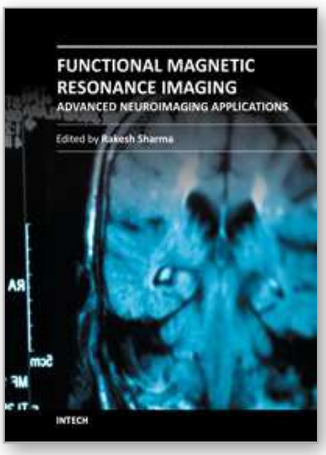

Functional Magnetic Resonance Imaging - Advanced Neuroimaging Applications

Edited by Prof. Rakesh Sharma

ISBN 978-953-51-0541-1
Hard cover, 206 pages
Publisher InTech
Published online 09, May, 2012
Published in print edition May, 2012

"Functional Magnetic Resonance Imaging - Advanced Neuroimaging Applications" is a concise book on applied methods of fMRI used in assessment of cognitive functions in brain and neuropsychological evaluation using motor-sensory activities, language, orthographic disabilities in children. The book will serve the purpose of applied neuropsychological evaluation methods in neuropsychological research projects, as well as relatively experienced psychologists and neuroscientists. Chapters are arranged in the order of basic concepts of fMRI and physiological basis of fMRI after event-related stimulus in first two chapters followed by new concepts of fMRI applied in constraint-induced movement therapy; reliability analysis; refractory SMA epilepsy; consciousness states; rule-guided behavioral analysis; orthographic frequency neighbor analysis for phonological activation; and quantitative multimodal spectroscopic fMRI to evaluate different neuropsychological states.

How to reference

In order to correctly reference this scholarly work, feel free to copy and paste the following:

Rakesh Sharma and Avdhesh Sharma (2012). Physiological Basis and Image Processing in Functional Magnetic Resonance Imaging: Neuronal and Motor Activity in Brain, Functional Magnetic Resonance Imaging - Advanced Neuroimaging Applications, Prof. Rakesh Sharma (Ed.), ISBN: 978-953-51-0541-1, InTech, Available from: http://www.intechopen.com/books/functional-magnetic-resonance-imaging-advanced-neuroimaging-applications/physiological-basis-and-imaging-processing-in-functional-magnetic-resonance-imaging-neuronnal-and-mo

INTECH
open science | open minds

InTech Europe
University Campus STeP Ri
Slavka Krautzeka 83/A
51000 Rijeka, Croatia
Phone: +385 (51) 770 447
Fax: +385 (51) 686 166
www.intechopen.com

InTech China
Unit 405, Office Block, Hotel Equatorial Shanghai
No.65, Yan An Road (West), Shanghai, 200040, China
中国上海市延安西路65号上海国际贵都大饭店办公楼405单元
Phone: +86-21-62489820
Fax: +86-21-62489821

IntechOpen